AD-A081 824 AIRESEARCH MFG CO OF CALIFORNIA TORRANCE F/G 7/1
HIGH-TEMPERATURE MECHANICAL PROPERTIES OF SINTERED ALPHA SILICO--ETC(U)
FEB 80 D M KOTCHICK N00014-76-C-0249
UNCLASSIFIED 80-16772 NL

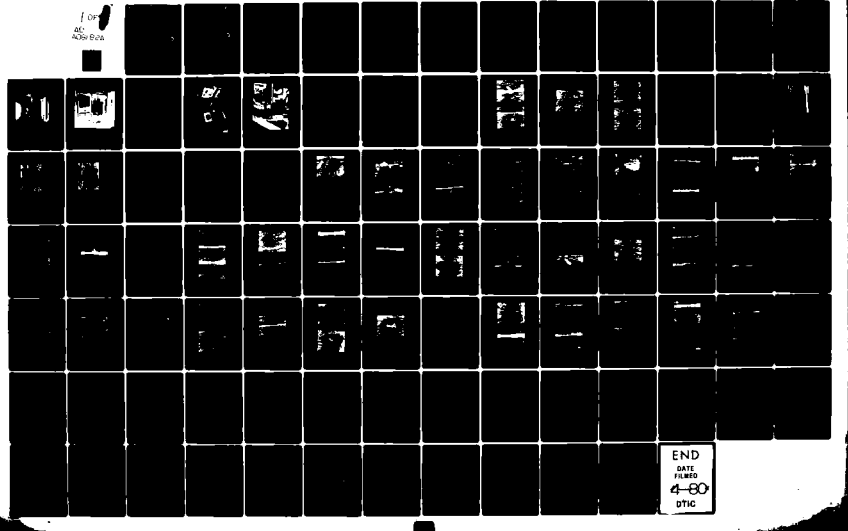

HIGH-TEMPERATURE MECHANICAL PROPERTIES OF SINTERED ALPHA SILICON CARBIDE (13 Oct 1978 - 13 Oct 1979)

80-16772

February 19, 1980

Research Sponsored by

Office of Naval Research
Department of the Navy

Under Contract N00014-76-C-0249

GARRETT

AIRESEARCH MANUFACTURING COMPANY
OF CALIFORNIA

AIRESEARCH MANUFACTURING COMPANY
OF CALIFORNIA

HIGH-TEMPERATURE MECHANICAL PROPERTIES OF SINTERED ALPHA SILICON CARBIDE

(13 Oct 1978 - 13 Oct 1979)

80-16772

February 19, 1980

Prepared by

M. Kotchick
Materials Engineering

for
Office of Naval Research
Department of the Navy

Under Contract N00014-76-C-0249

Approved: W. S. Miller
W. S. Miller
Program Manager

Approved: N. J. O'Reilly
N. J. O'Reilly
Chief Engineer
Heat Transfer and
Cryogenic Systems

ACKNOWLEDGEMENTS

This report was prepared by David M. Kotchick, principal investigator of the materials engineering group. William S. Miller of the heat transfer and cryogenic systems group served as program manager. The high-temperature testing and SEM analysis was conducted at AiResearch by Pat Patterson.

Mr. Keith Ellingsworth of the power program, material sciences division, Office of Naval Research, was the technical monitor on the program. His guidance and support are deeply appreciated.

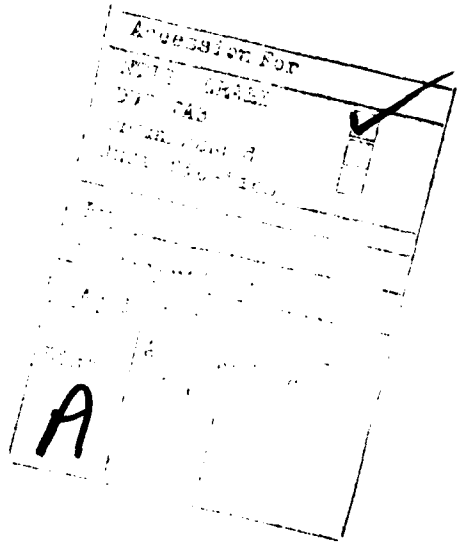

CONTENTS

SECTION 1

INTRODUCTION

This report summarizes the results of the fourth year of a continuing research program on the various grades of silicon carbide of interest for naval applications. This program has thus been designated as ONR-4.

During the ONR-2 program[1]* some of the important basic mechanical properties of sintered alpha silicon carbide were investigated. At that time an extensive literature survey was conducted and included as part of the ONR-2 annual report. Since that time one particularly significant program investigation was concluded on the effects of oxidation on slow crack growth (SCG) in sintered alpha silicon carbide (SASC). In this study by McHenry[2] it was shown that when the oxide layer was removed from high-temperature preoxidized SASC samples it exhibited SCG at temperatures and oxygen partial pressures where this phenomena had not previously been detected. This result indicated that surface oxidation of SASC has some effect on the bulk properties (probably by changing the grain boundary chemistry), which causes the enhancement of SCG. SCG was not found in SASC in inert atmospheres previous to oxidation.

The ONR-3 program was initiated to further explore the limitations of SASC in oxidizing and marine (salt-bearing) environments as a function of reliability, particularly for use in high-temperature heat exchangers and turbines. The program was also formulated to generate stressed-lifetime data using differential strain rate techniques. These data can be generated by stress rupture testing, but it is a time consuming procedure. If there is little or no crack growth for the particular testing environment during stress rupture testing, the time to failure is either very long or occurs within a very narrow stress interval. To minimize the need to collect stress rupture data, the same information can be generated from other types of tests. This approach is based on the fracture mechanics theory that fatigue failure of ceramics occurs from stress-dependent growth of preexisting flaws to dimensions critical for spontaneous crack propagation. Furthermore, using expressions developed for time-to-failure predictions, the life expectancy of parts under a particular cyclic loading schedule can be predicted from static (stress rupture) or dynamic testing experiments. The most reliable stressed-lifetime predictions would be those generated from a combination of static, dynamic, and cyclic testing, since the operating components will be subjected to loading that is simulated by these three types of tests.

The results of ONR-2 and ONR-3 were in good agreement for the strength versus temperature relationships investigated. Strain rate experiments and calculated values agreed with the results of McHenry[2] that SASC is susceptible to SCG after oxidation. At 1550°C the strength of SASC begins to decrease significantly, indicating a maximum long-time use temperature. Coating and fusing ocean salt onto the surface of oxidized samples seemed to have little effect on the fracture stress. Fused salt coatings on as-received specimens seemed to decrease the fracture stress at 1275°C, but at 1550°C the fracture

*See Section 7 for references.

stresses are similar to those for oxidized samples. Since more specimens were tested in ONR-3 for each test condition, the results of the life prediction were more significant than ONR-2 and therefore a better indication of the material properties, especially Weibull modulus.

The ONR-4 program was undertaken to determine the type of flaws that were causing failure of specimens tested in the ONR-2 and ONR-3 programs. A scanning electron microscope was used to examine the fracture surfaces of all the specimens and to classify the type of defects causing failure. Special attention was to be focused on the effects of oxidation and salt on the failure causing defects.

SECTION 2

BACKGROUND

During the ONR-2 program a test plan was followed that helped to determine the stress-lifetime-reliability diagram as a function of temperature for samples of sintered alpha silicon carbide with as-fired surfaces and as-fired and salted surfaces. The test plan for ONR-3 was based on the results of ONR-1 and ONR-2, as well as data generated on SASC at Penn State and Rockwell Science Center. The collective data of these programs allows a reasonable determination of the rate of subcritical crack growth in this material, which is important design data for future Naval applications. It also has the objective of identifying those critical parameters that limit or degrade the strength of SASC.

The prediction of stressed-lifetime for ceramics is based on the growth of preexisting cracks under stress to a critical size where catastrophic failure occurs by spontaneous crack growth (energetically favored crack extension). From fracture mechanics theory, the stress intensity/crack velocity diagram (K/V) is of critical importance for lifetime prediction. Figure 2-1 is a schematic representation of the ideal K/V diagram. The stress intensity factor, K, is usually expressed as $K = \sigma(YC)^{1/2}$ for ceramics where σ = stress, C = crack length, and Y = a geometrical factor. In region I, the rate of reaction between the corrosive species and the atoms under stress at the crack tip is controlling. In region II, the diffusion of corrosive species to the crack tip is rate controlling Region III expresses the crack growth independent of the environment, since the crack would be traveling faster than the diffusion of the corrosive species.

This type of data can be generated from crack propagation tests of large preformed cracks by the double torsion method. Determination of K/V slope by double torsion methods may not be characteristic of crack propagation of inherent surface flaws, which usually are the cause of failure in ceramics since the double torsion experiment yields data from a macroscopic crack.

In regions I and III, the slope of the K/V diagram, n, can be determined from the ratio of strengths (σ) at two strain rates ($\dot{\varepsilon}$) by

$$\left(\frac{\sigma_1}{\sigma_2}\right)^{n+1} = \left(\frac{\dot{\varepsilon}_1}{\dot{\varepsilon}_2}\right) \qquad (1)$$

The value of n can then be used to define the relation between the failure time in a constant strain rate test, $\tau_{\dot{\varepsilon}}$, and the failure time under the maximum stress obtained in a constant stress test, $\tau_{\dot{\sigma}}$, using

$$\tau_{\dot{\sigma}} = \frac{\tau_{\dot{\varepsilon}}}{n+1}$$

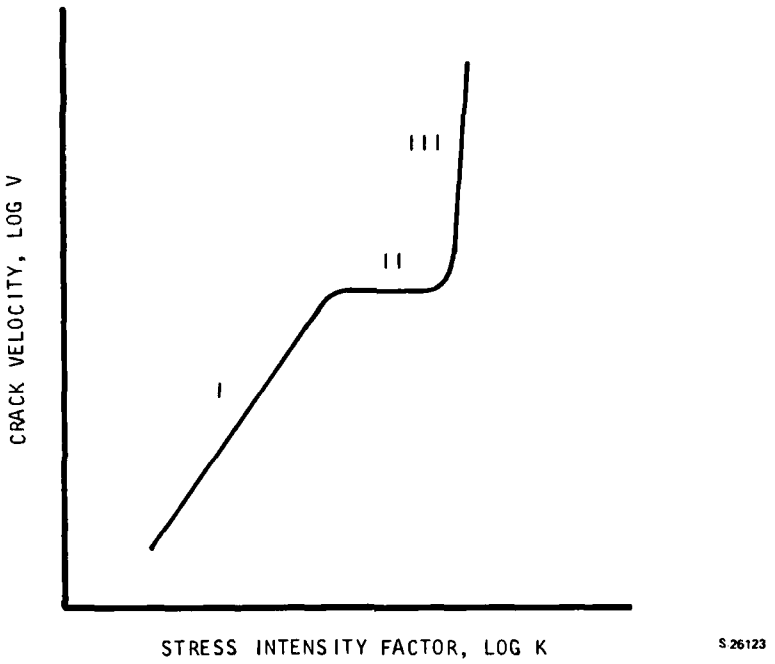

Figure 2-1. Schematic Representation of Ideal K/V Diagram

The probability of failure of ceramics can be most accurately characterized by means of the standard Weibull statistics expression as

$$S = 1 - \exp\left[-V\left(\frac{\sigma_f}{\sigma_o}\right)^m\right] \qquad (3)$$

Where S is the failure probability, V is the stressed volume of surface area depending on the type of flaws causing failure, σ_f is the fracture stress, σ_o is the characteristic stress (which is a normalizing constant), and m is the Weibull modulus. The fracture strengths of a group of samples can be used to estimate m and σ_o when Equation (3) is rewritten as

$$\ln \ln \frac{1}{1-S} = \left\{\ln V - m \ln \sigma_o\right\} + m \ln (\sigma_f) \qquad (4)$$

The value of S can be estimated from S - s/n + 1 where n is the total number of samples in a test and s is the number of the sample when the group is arranged in increasing order of fracture stress. When ln ln (1/1-S) is plotted versus ln σ_f, m is the slope.

The ratio of failure times at different applied stresses can be written as

$$\left(\frac{\sigma_1}{\sigma_2}\right)^n = \left(\frac{\tau_2}{\tau_1}\right) \qquad (5)$$

Using this relation, data from the experimentally determined failure probability curve can then be used to predict the family of failure probability curves as a function of time to failure, which can be used to predict stressed lifetime. If the time to failure of samples tested at greatly different strain rates ($\Delta > 10^2$) is used to predict the failure probability at long lifetimes, it is possible that a refinement of the prediction can be made, provided that subcritical crack growth is occurring at all the strain rates tested.

SCG studies on SASC have until recently shown that SCG did not exist below 1500°C [6,7,8] (except in water). Preoxidation has recently been shown to enhance SCG in SASC[2]. The results of ONR-2 and ONR-3 show evidence of SCG as low as 1200°C on oxidized specimens.

SECTION 3

EXPERIMENTAL PROCEDURE

MATERIALS

Billets of SASC manufactured by Carborundum Company were prepared by cold-pressing and sintering. The flexure bars were 2.5 x 5 x 44 mm. Each of the specimens were cut from the top surface of SASC billets, leaving the top face as-formed and as-fired. The bottom face of each sample was ground with 200-grit diamond and then finished with 400-grit diamond. Long edges were lightly chamfered by hand with 220-grit diamond lapping compound. Width and thickness were within 0.13 mm of specified values. Ground surfaces were flat within 25 μm. Ground sides were parallel within 25 μm and were perpendicular to the faces within 1°. Visual, fluorescent dye-penetrant and radiographic inspections ensured that each specimen was free of defects greater than 0.5 mm long. Density, measured by the immersion method (ASTM-C373-72) varied from 3.08 to 3.15 g/cc.

For each test, specimens were randomly selected from among those that passed inspection so that the variations due to composition and processing differences would influence all the test groups in the same way. All specimens were tested on the as-fired face since most components for heat exchanger use would be used in the as-fired condition with little or no elaborate surface treatment.

Tables 3-1 and 3-2 outline the experimental test plan and results for ONR-2 and ONR-3, respectively. Indicated are the sample test condition, assigned group number, test temperature, test displacement rate, number of specimens tested, median stress, mean stress, standard deviation, and Weibull modulus (m). The oxidized samples were treated for 24 hours at 1260°C in air so that weight gain by oxidation was past the initial rapid reaction to a point of constant weight gain with time. This schedule was selected after consideration of oxidation experiments conducted on SASC by Costello and Tressler[3]. The salt-treated samples were cleaned with isopropanol and coated with concentrated antificial ocean saltwater (ASTM-D1141-52 (without heavy metals)), baked in air at 900°C for 65 hr and then at 1260°C for 65 hr in an electric furnace.

Flexure tests were conducted in a SASC floating-pin, 4-point bend fixture (Carborundum Company) having a 38-mm outer span and a 13-mm inner span (Figure 3-1). Loads were applied by a universal test machine (Instron Corp.) at varying displacement rates through silicon carbide push rods (Figure 3-2). Loading rates, recorded autographically, were converted to strain rates through the equation

$$\dot{\varepsilon} = \frac{1.5\,\dot{L}}{WH^2\,E}$$

where $\dot{L}$ is the recorded load rate, W is the specimen width, H is the specimen thickness, and E is the elastic modulus. A value of 414 GPa (60 Mpsi) was used for E at all temperatures, based upon available data[4,5].

TABLE 3-1

GROUP RESULTS FOR ONR-2

Sample Condition	Group No.	Temp., °C	Displacement Rate, in./min	No. Tested	Mean Stress, ksi	Standard Deviation, ksi	Median Stress, ksi	Weibull, m
A-As Rec	1	20	0.02	19	49.6	6.9	50.2	7.7
A-As Rec	2	1060	0.0002	5	56.9	6.1	57.3	8.0
A-As Rec	3	1340	0.02	5	54.9	5.7	55.3	8.2
A-As Rec	4	1340	0.0002	6	50.5	5.9	50.9	7.6
A-As Rec	5	1620	0.02	6	33.9	3.6	34.2	8.2
A-As Rec	6	1620	0.0002	6	26.6	2.7	26.8	9.1
A-O	7	20	0.02	9	58.5	7.0	59.0	8.0
A-O	8	1340	0.02	8	53.2	6.4	53.7	7.5
A-O	9	1340	0.0002	9	46.6	5.7	47.1	7.8
A-O	10	1620	0.0002	4	30.9	5.2	31.0	-
A-S	11	20	0.02	10	54.1	7.7	54.6	6.8
A-S	12	1060	0.0002	5	53.6	4.4	53.9	10.1
A-S	13	1340	0.02	9	56.6	5.8	57.1	9.4
A-S	14	1340	0.002	6	51.7	8.5	52.2	5.2
A-S	15	1340	0.0002	9	44.0	5.6	44.4	7.4
A-S	16	1620	0.02	6	33.0	3.0	33.2	10.1
A-S	17	1620	0.002	1	26.6	-	-	-
A-S	18	1620	0.0002	5	26.3	4.4	26.5	4.8
G	19	20	0.02	7	50.7	3.4	51.0	13.7
G	20	1340	0.02	5	55.6	6.2	56.1	7.4
G	21	1620	0.0002	1	27.9	-	27.9	-
G-S	22	20	0.02	1	52.2	-	52.2	-
G-S	23	20	0.0002	8	49.3	9.7	49.7	4.5
G-S	24	1340	0.02	5	52.2	8.4	52.6	5.3
G-S	25	1340	0.0002	10	48.4	8.6	48.9	5.4
G-S	26	1620	0.02	5	36.3	5.6	36.6	5.7
G-S	27	1620	0.0002	5	23.1	2.0	23.2	9.5

A = As Fired
O = Oxidized
S = Salt Treated
G = Ground (transverse to long axis)

TABLE 3-2

GROUP RESULTS FOR ONR-3

Sample Condition	Group No.	Temp., °C	Displacement Rate, in./min	No. Tested	Mean Stress, ksi	Standard Deviation, ksi	Median Stress, ksi	Weibull, m
A-As Rec	100	20	0.02	10	43.8	3.6	44.1	11.9
A-O	101	20	0.02	10	54.4	4.2	54.8	12.3
A-O	102	20	0.0002	9	50.3	5.0	50.9	7.1
A-O-Dry N_2	103	20	0.0002	10	56.2	3.9	56.6	13.2
A-O	104	1550	0.02	10	47.1	7.6	47.6	5.9
A-O	105	1550	0.002	5	43.7	5.2	44.0	6.8
A-O	106	1550	0.0002	10	34.1	4.9	34.4	6.7
A-O	107	1275	0.02	5	54.3	7.6	54.7	6.1
A-O	108	1275	0.002	5	52.4	8.9	52.8	4.5
A-O	109	1275	0.0002	5	49.1	2.1	49.4	17.6
A-O	110	1000	0.02	5	55.4	2.7	55.6	17.7
A-O	112	1000	0.0002	10	51.9	10.8	52.4	4.7
A-O-S	113	1550	0.02	8	48.2	5.7	48.7	7.9
A-O-S	114	1550	0.0002	6	35.8	5.4	36.1	5.7
A-O-S	115	1275	0.02	7	57.1	5.8	57.6	9.1
A-O-S	116	1275	0.0002	8	53.2	4.8	53.6	10.2
A-S (Not preoxidized)	117	1550	0.02	7	50.6	9.1	51.1	5.1
A-S (Not preoxidized)	118	1550	0.0002	8	32.9	4.8	33.2	6.3
A-S (Not preoxidized)	119	1275	0.02	8	53.5	7.6	54.0	6.5
A-S (Not preoxidized)	120	1275	0.0002	8	44.5	7.9	44.8	5.3

A = As Fired
O = Oxidized
S = Salt Treated

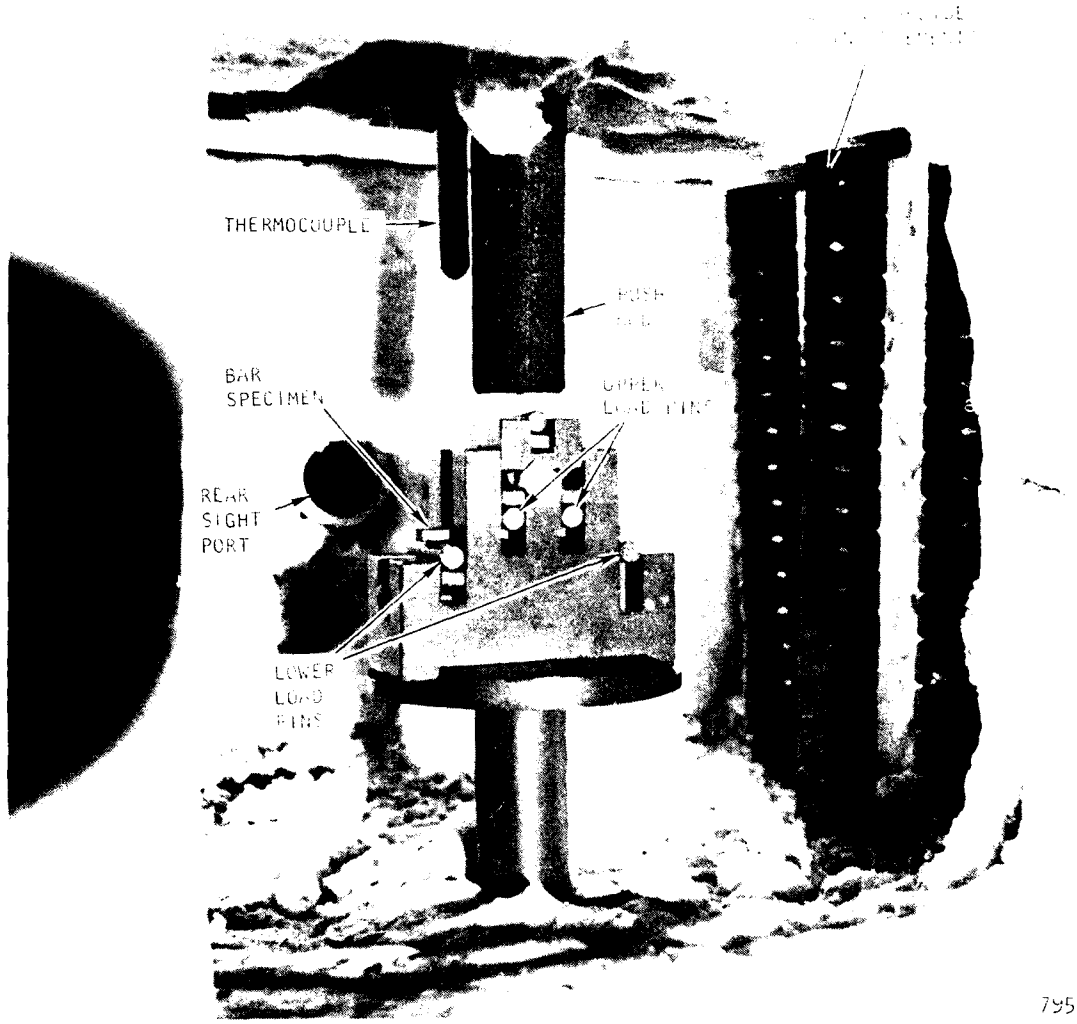

Figure 3-1. Four-Point Bar Flexure Strength Apparatus

79593-4

F-31384

Figure 3-2. Instron with High Temperature Furnace

The fixture and specimen were contained within a silicon carbide element electric furnace (W.P. Keith Co.), which provided temperatures as high as 1620°C. Temperatures were monitored with a micro-optical pyrometer and were within 3°C of the reported value.

Fracture surfaces of each specimen were examined under low-magnification stereomicroscope to locate the fracture origin. Traceability of specimens was maintained.

The results of the program were summarized in "High Temperature Strength of Sintered α-SiC in Salt and Oxidizing Environments". The paper was submitted and accepted for publication in the Bulletin of the American Ceramic Society (see Appendix A).

Fractured specimens were cleaned, coated, and examined for various failure characteristics on the scanning electron microscope (SEM), shown in Figure 3-3. All specimens mechanically tested during the ONR-2 and ONR-3 programs were considered for SEM analysis. Some specimens were broken into very small pieces from high-energy fracture that could not be used for fracture analysis. The remaining specimens were first examined using a low-magnification stereomicroscope to locate the fracture surface. Several pieces often resulted from the flexure tests. The specimens were cleaned in isopropanol using an ultrasonic bath and dried in a vacuum drying oven. The two halves of the fractured specimen were mounted with their tensile-tested faces together, which made it easier to identify the origins. A specially-designed carousel sample holder was constructed to allow easy analysis of eight fractured specimens without removing the fixture from the SEM vacuum chamber. The carousel and samples were shadow-coated with electrically deposited gold to prevent electrical charging of the nonconducting oxide or salt-coated surfaces. The loaded carousel is shown in Figure 3-4.

Initial SEM inspection of the fractured specimens was used to collect information about the type of failures and flaw characteristics. The examined specimens were classified as to the location of the critical flaw (surface, subsurface, corner, or tensile face), the type of flaw (inclusion, pore, low-density area, pit, etc.), and flaw size. Any special characteristics were noted, such as intergranular fracture. This data was then compiled with regard to test conditions and used to direct selected analyses. X-ray analysis in the SEM was used to look for salt contamination in near-surface pores and cracks and to examine the composition of inclusions.

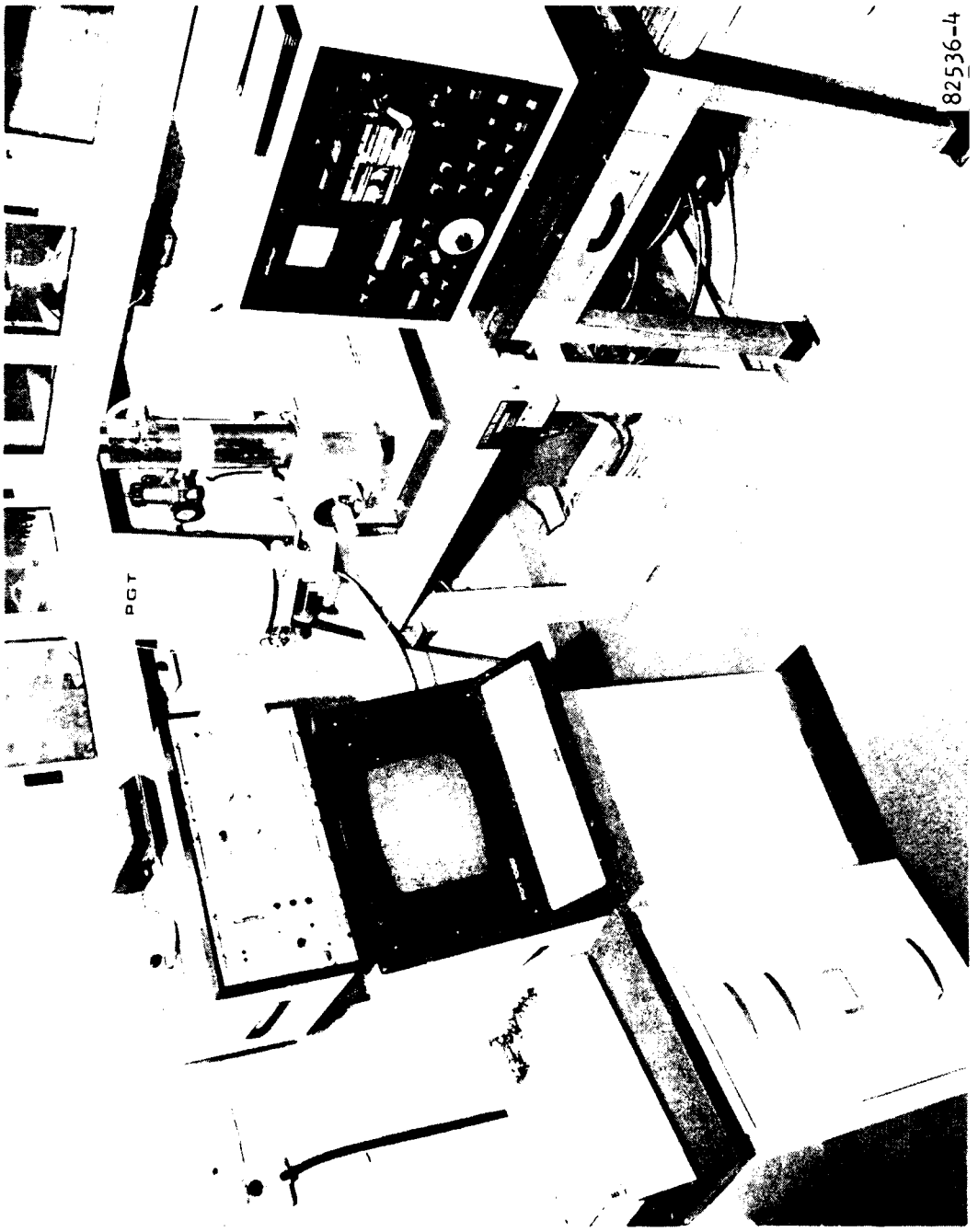

Figure 3-3. Scanning Electron Microscope Including X-Ray Analysis

F-31378

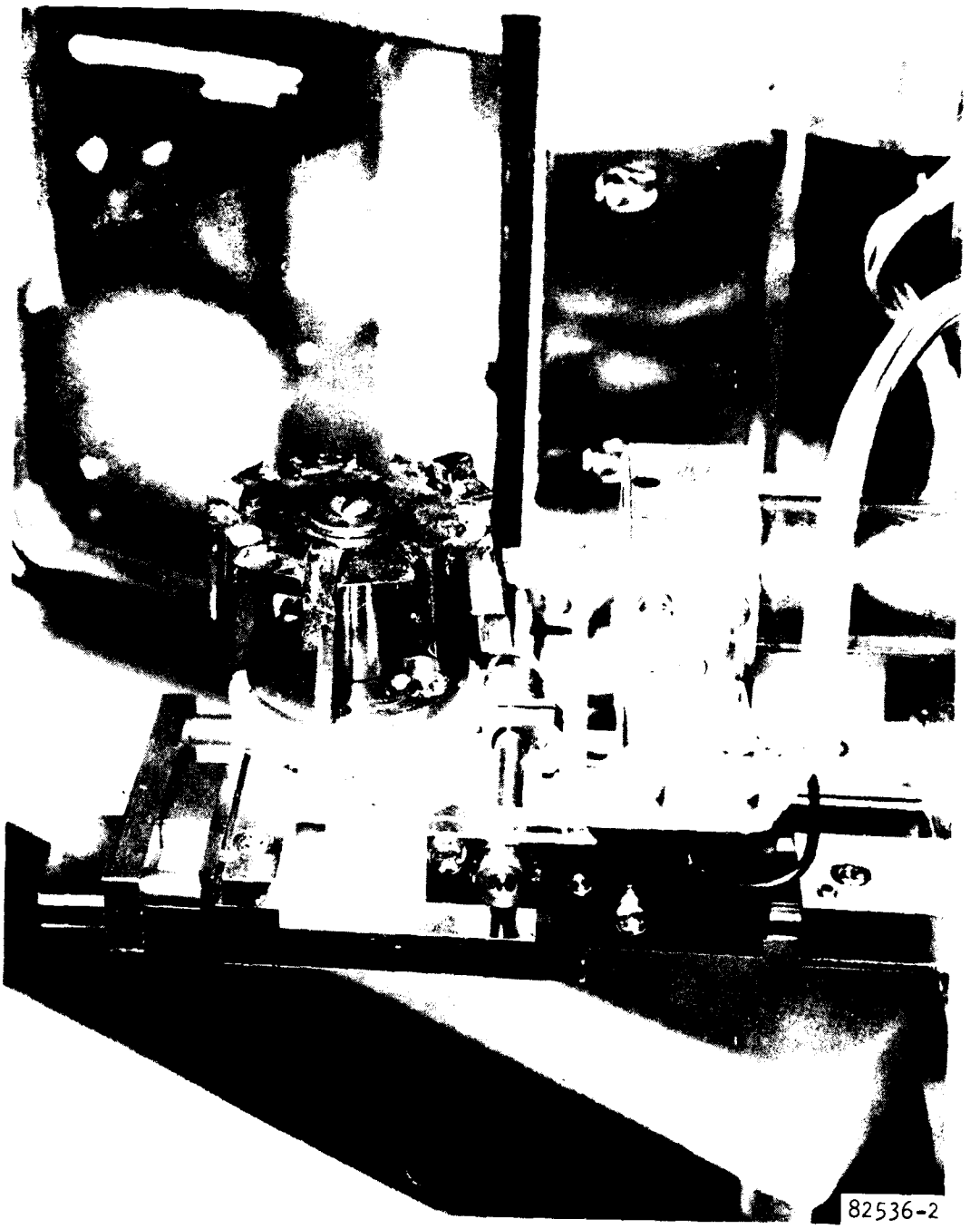

F-31379

Figure 3-4. Loaded Specimen Carousel on the SEM Stage

SECTION 4

RESULTS

Of 338 mechanically-tested specimens, 290 were examined and photographed in detail on the scanning electron microscope. Over 1200 photomicrographs were processed. Tables 4-1 and 4-2 summarize the results. Note that many of the classifications are subjective and could vary for different observers. To keep such variations to a minimum, a series of examples was established to aid in the classification process.

When possible, the location of the strength limiting flaw was determined from the SEM micrographs. This location was classified as either surface or subsurface, surface flaws having some part of the flaw touching the specimen surface and subsurface flaws being completely enclosed within the body of the specimen. Corner failures were classified as to the surface or subsurface flaws that touched the chamfered edge of the specimen or were enclosed within the specimen body just below the chamfered surface. All other locations were classified as tensile face failures.

Several special types of defects were identified as the critical flaws in a large percentage of the specimens. Pits (pores open to the surface) and pores (subsurface voids) were classified together (Figure 4-1). Low-density areas (Figure 4-2) were classified as such when compared to the surrounding microstructure. Flat plate-like cracks (Figure 4-3) running parallel to the tensile surface were usually found grouped several to a cluster and were termed flake-like pores. Inclusions (Figure 4-4) were termed as any material within the matrix that appeared to be foreign to the matrix. In a few cases surface scratches and cracks could be identified. If the strength limiting defect could not be identified, the origin was termed uncertain.

Table 4-3 is a summary of the type of defects that caused failure in both ONR-2 and ONR-3 programs. The percentage of samples that could be examined by SEM was restricted in the case of the ONR-2 program (77.2 percent), since a large number of these specimens broke into very small pieces during fracture. A high percentage of the specimens tested in ONR-3 (95.6 percent) were SEM examined.

Of the specimens that were examined by SEM, specimens tested in the ONR-2 program had a higher percentage (89.2) of failures originating from the surface than in the ONR-3 program (79.5). The ratio of corner failures to tensile face origins was slightly higher for ONR-2. The difference is small and this ratio can probably be considered the same in both programs.

The size of defects observed in both programs is quite different. In ONR-2, a significantly larger percentage of defects (25.9 percent) less than 25μm in size was observed than in ONR-3 (12.3 percent). The number of defects between 25 to 100 μm is nearly the same for both programs. The percentage of defects greater than 100 μm is significantly greater for the ONR-3 program (38.4) over ONR-2 (27.3). These results indicate that since the average flaw size was larger for ONR-3, the average fracture energy was also lower and may be the reason more of the ONR-3 specimens did not shatter into small pieces as a result of the flexure tests.

TABLE 4-1

SUMMARY OF SEM ANALYSIS FOR ONR-2 SPECIMENS

Rod	Total No. Samples Tested	No. [illegible] SEM Analysis	No. Speci-mens Not Examined	No. Surface Origins	No. Corner Origins	No. Face Origins	Flaw Size [illegible] 25	25 to 100 [illegible]	[illegible]	Flake-Like Pore	[illegible]	Pit or Pore	Uncer-tain	Rack	Scratch	Corrosion	Note	SCG	Test Temp., °F	Surface Cond., (A, S, [illegible])	[illegible]	Cross-head, [illegible]
1	19	[illegible]	11	5 (3)	1	7	4	1	3	1	5								RT	A		[illegible]
2	5	5		4 (1)		5		4	1		2	5							[illegible]	A		[illegible]
3	5	5		5	1	4	3	1	1			1	2	1			1		1340	A	1	0.02
4	6	6		6		6	2	2	2		2	2	2						1340	A		[illegible]
5	6	6		6	2	4	2	1	3		3	2	1				[illegible]	[illegible]	[illegible]	A		[illegible]
6	6	6		6		6	3		2		1		4				6	6	1620	A		0.0002
7	10	5	5	4 (1)		5	3		2			3	2						RT	AC	1	0.02
8	8	5	3	4 (1)	2	3	1	1	3		4	3		1			1		1340	AC		0.02
9	9	6	3	5 (1)	1	6	1	3	2	1	[illegible]	3		[illegible]			[illegible]		1340	AC		0.0002
10	4	1	3	1		1			1		1						1		1620	AC		0.02
11	10	10		8 (2)		10	3	5	2			5	1	1	1		1		20	AS	2	0.02
12	5	5		5	1	5		4	1		2	3							1060	AS		0.0002
13	9	4	5	3 (1)	1	3		3	1		1		1	1	1		1		1340	AS		0.02
14	6	3	3	3		3		2			3	1							1340	AS		0.02
15	10	3	7	3		3		3			3						1		1340	AS		0.0002
16	6	6		6		6	2	1	2		4		2			6	3	5	1620	AS		0.02
17	4	4		4	1	3		1	3	1	2	1					3	3	1620	AS		[illegible]
18	5	5		5	2	3		4	1								5	5	1620	AS		0.0002
19	7	7		5 (2)		7	5	2			2	3		4					RT	G	1	0.02
20	5	5		2 (2)	1	3		3	1		1	3	1				1		1340	G		0.02
21	1	1		1		1		1										1	1620	G		0.0002
22	1	1		0 (1)		1		1				1							RT	GS		0.02
23	8	8		5 (3)	1	7		4	3		2	5		1			1		RT	GS		0.0002
24	5	5		5		5	1	4			2	2	1	1					1340	GS		0.02
25	10	9	1	9	1	8	5	2	2		4	1		2			6	6	1340	GS		0.0002
26	5	5		4 (1)		5	1	3	1		1	1	2	2			1		1620	GS		0.02
27	5	5		5	3	3		4	1				2				4	4	1620	GS		0.0002
Total	180	139	41	119 (19)	18	123	36	60	39	3	45	48	24	16	2	6	40	32			[illegible]	

TABLE 4-2

SUMMARY OF SEM ANALYSIS FOR ONR-3 SPECIMENS

Run No.	Total No. Samples Tested	[illegible] SEM Analysis	No. Specimens Not Examined	No. Surface Origins (Subsurface)	No. Corner Origins	[illegible]	Flaw Size <25 μm	Flaw Size 25 to 100 μm	Flaw Size >100 μm	Flake-Like Pore	Low Density	Pit or Pore	Uncertain	Crack	Scratch	Corrosion	Note	SCC	Test Temp., °C	Surface Cond., (A, S, [illegible])	Inclusion	Cross-head, in./min
100	10	8	2	7 (1)		8	3	1	3	2	2	3	3						RT	A	1	0.02
101	10	10		3 (7)	1	9		8	1	2	3	8							RT	AS	2	0.02
102	10	10		3 (7)	3	7		5	5	3	3	6		1			1		RT	AS	2	0.0002
103	10	10		1 (9)		10	2	6	3	1	1	8							RT	AS AS	5	0.0002
104	10	10		5 (5)	1	9		5	5	4	5	7							1550	AS		0.02
105	5	5		2 (3)		5		1	4		5	1						2	1550	AS		0.002
106	10	10		9 (1)	1	9	3	5	2		1	3	6	1				7	1550	AS		0.0002
107	5	5		3 (2)	2 (2)	3		3	3	1	2	4					1		1275	AS		0.02
108	5	5		5		5		2	3	2		3							1275	AS		0.002
109	5	5		2 (3)		5		2	3	4	3	2							1275	AS		0.0002
110	5	5		1 (4)		5		4	1		2	5							1000	AS		0.02
112	10	10		9 (1)		10	1	2	7	3	2	9					1		1000	AS		[illegible]
113	[illegible]	8		6 (2)	1	8	1	2	5	3	6	2					1	2	1550	ACS		0.02
114	8	6	2	4 (2)	1	5	1	4	1	1	1	2	1	1	1			6	1550	ACS		0.0002
115	8	8		5 (3)		8		4	4	2	2	6							1275	AS		[illegible]
116	8	5		6 (1)		7	2	4	1		4	5	3				1		1275	AS	1	[illegible]
117	7	4	3	3 (2)		4		1	2		2	3	1				2	2	1550	AS		[illegible]
118	8	8		6 (2)	1	7	2	3	2	2	1	2	4		1		7	6	1550	AS		[illegible]
119	8	8		4 (4)	2	6	2	5	1	2	1	5	1			1			1275	AS		0.02
120	8	8		5 (3)		8	2	4	2	1	4	5							1275	AS		0.0002
Total	158	151	7	[illegible] (62)	12 (2)	138	19	61	58	33	50	69	19	3	2	1	14	25			[illegible]	

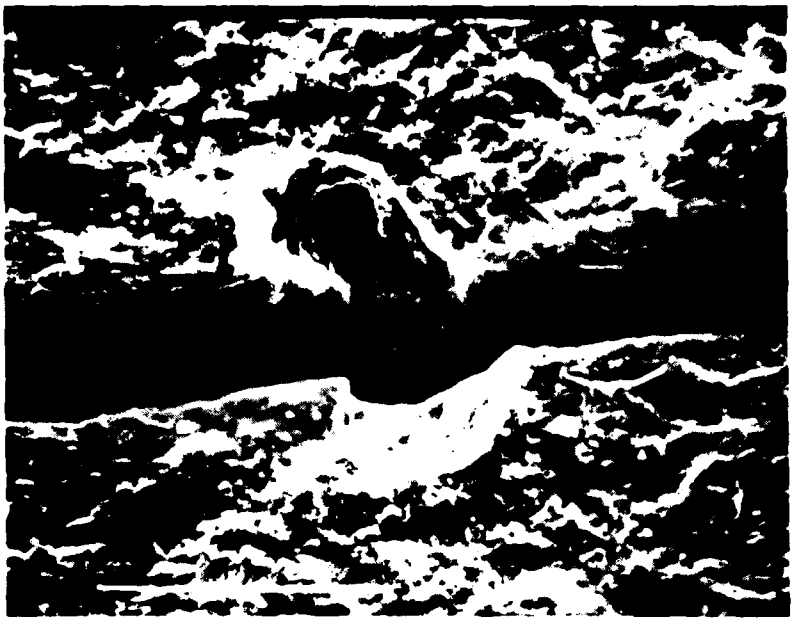

a. ONR-3, GROUP 115, 350X

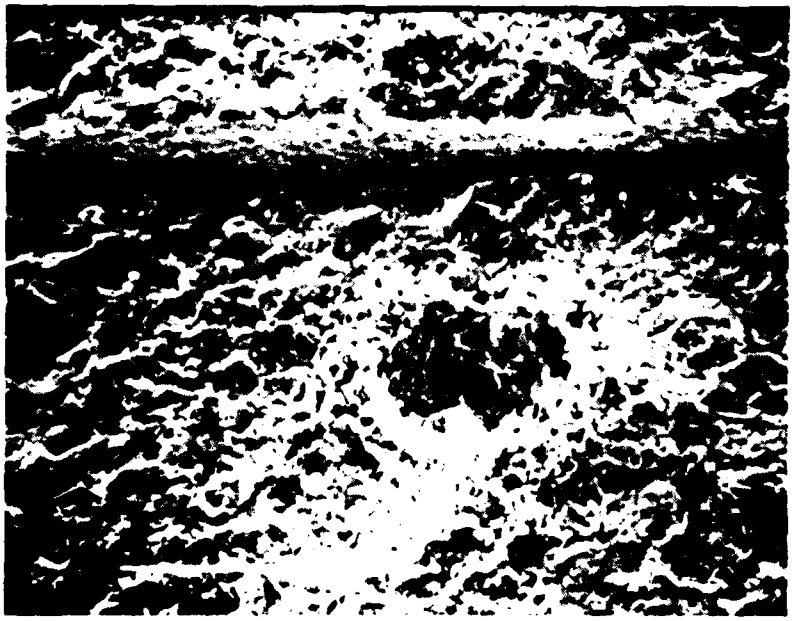

F-31318

b. ONR-2, GROUP 20, 350X

Figure 4-1. Typical Pit (ONR-3, Group 115, 350X) and Pore (ONR-2, Group 20, 350X) Found as Failure Origins in SASC

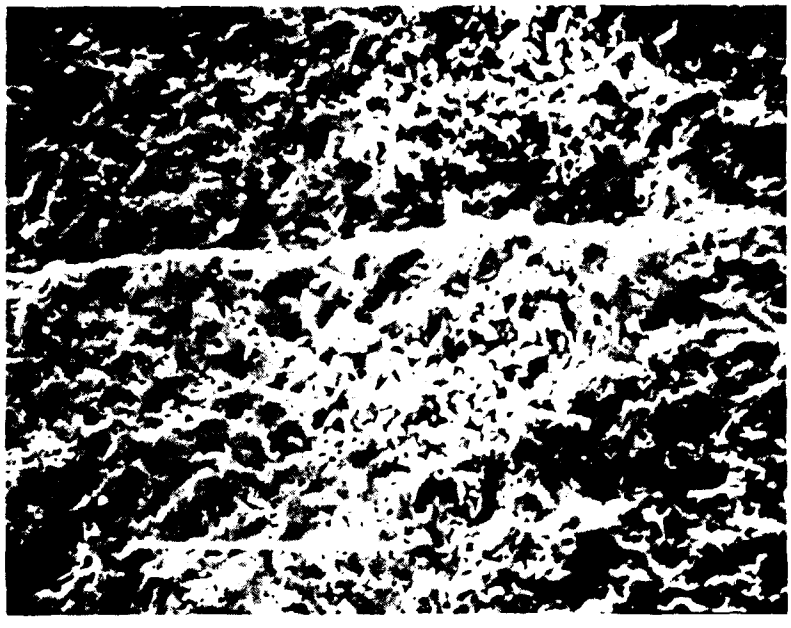

F-31319

Figure 4-2. Typical Low-Density Area Found as a Failure Origin in SASC (ONR-2, Group 9, 350X)

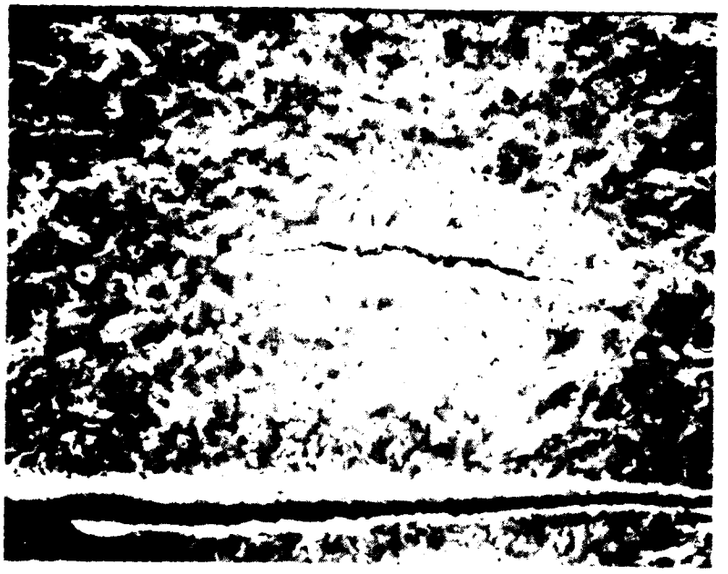

F-31320

Figure 4-3. Typical Plate-Like Cracks Found as a Failure Origin in SASC (ONR-3, Group 109, 350X)

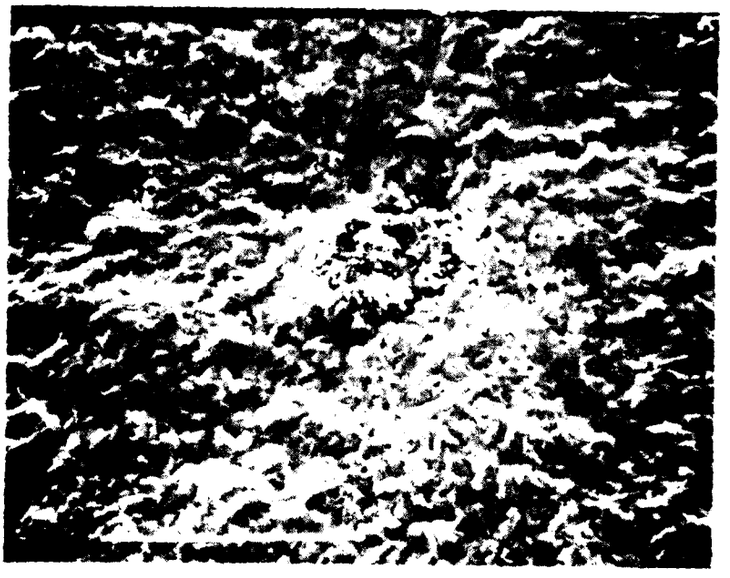

F-31321
F-31380

Figure 4-4. Typical Inclusion Found as a Failure Origin in SASC (ONR-3, Group 103, 350X)

TABLE 4-3

PERCENTAGES OF VARIOUS FAILURE ORIGINS

	ONR-2	ONR-3
Percent of samples tested and SEM examined	77.2	95.6
Percent of samples SEM examined with:		
Surface origins	89.2	79.5
Corner origins	12.9	7.9
Face origins	88.5	91.4
Defects less than 25 μm	25.9	12.3
Defects between 25 to 100 μm	43.2	40.4
Defects greater than 100 μm	27.3	38.4
Flake-like pores	2.2	21.9
Low-density origins	32.4	33.1
Pits or pores for origins	34.5	58.9
Uncertain origins	17.3	12.6
Cracks for origins	11.5	2.0
Scratches for origins	1.4	1.3
Intergranular fracture near the origin	23.0	16.6
Percent of samples SEM examined and tested at:		
1620°C showing intergranular fracture	66.7	
percent at 0.0002 in./min	94.1	
1550°C showing intergranular fracture		49.0
percent at 0.0002 in./min		79.2
1340°C showing intergranular fracture	11.8	
percent at 0.0002 in./min	25.0	
1275°C or less showing intergranular fracture	0.0	0.0

The types of flaws identified as failure origins varied from program to program. The major difference was in the flake-like flaws that were identified in 21.9 percent of the ONR-3 specimens, but in only 2.2 percent of the ONR-2 specimens. A similar number of specimens failed at lowdensity regions in both programs. A significantly larger number of specimens failed at pits or pores in ONR-3 (58.9 percent) than in ONR-2 (34.5 percent). In the ONR-2 program, a greater number of specimens (11.5 percent) could be identified as having failed from pre-existing surface cracks.

A large number of specimens from both programs (23 percent in ONR-2 and 16.6 percent in ONR-3) could be identified as having intergranular fracture near the origin. These groups were broken down into subgroups according to test temperature and testing displacement rate. All observations of intergranular fracture occurred above 1275°C with an increasing number of observations with increasing test temperature. The percentages calculated at 0.0002 in./min in Table 4-3 include only specimens tested at this displacement rate and indicated temperature.

The dispersive X-ray analysis capabilities of the SEM were used in an attempt to identify the composition of inclusions and the composition in the area of the strength controlling defect. Figures 4-5, 4-6, and 4-7 show the X-ray spectrums of the fracture surfaces of three samples tested at 1550°C and 0.0002 in./min. The surface conditions were AOS (as-fired, oxidized, and salted), AO (as-fired and oxidized), and AS (as-fired and salted), respectively. No detectable compositional difference was found at the fracture origins. The analysis of what appeared to be inclusions (see Figure 4-4) showed no detectable difference from the matrix to at least the limit of the X-ray analysis.

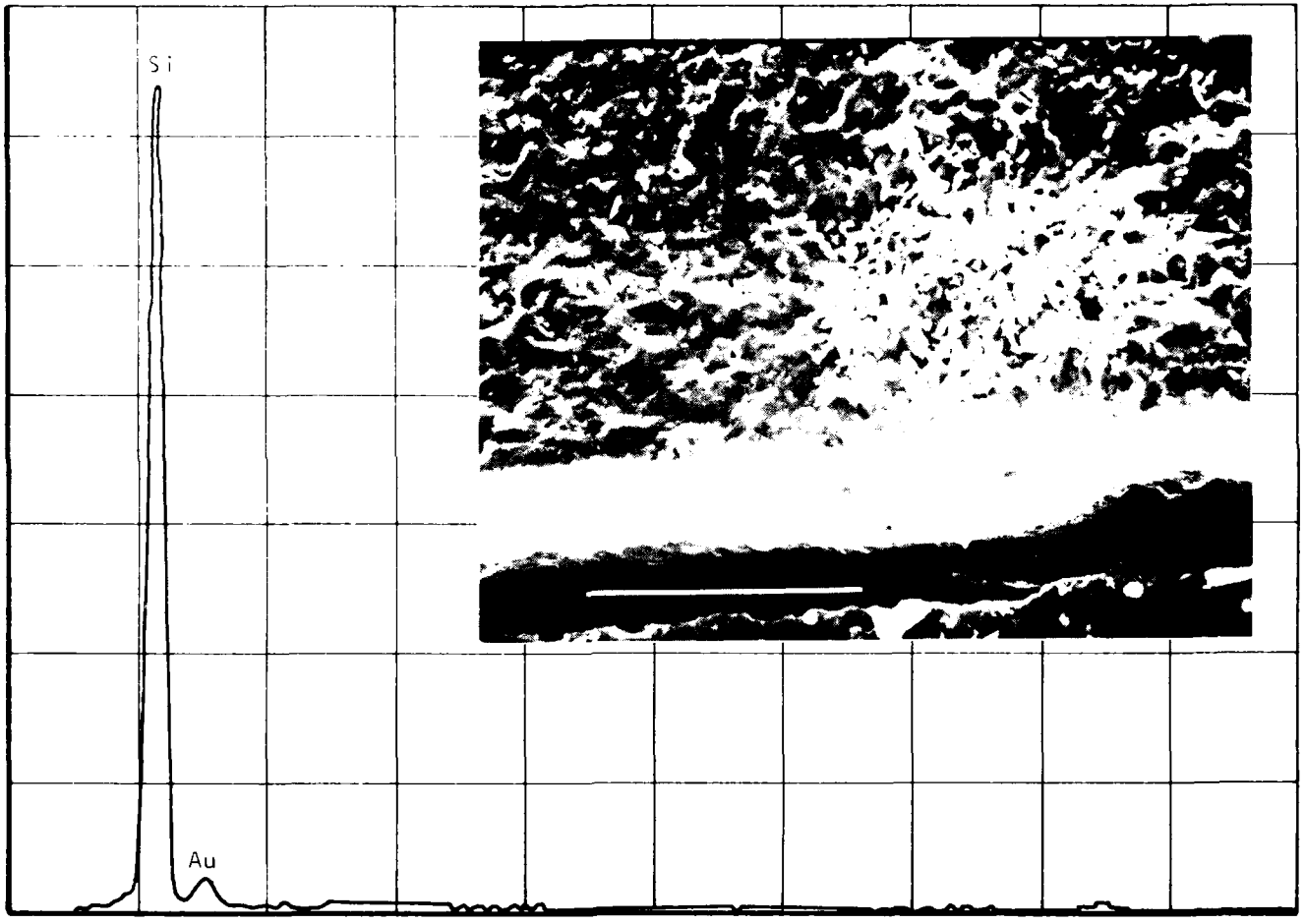

Figure 4-5. X-Ray Spectrum at the Point of Intergranular Fracture and SEM Micrograph for Sample 37, Group 114 (350X)

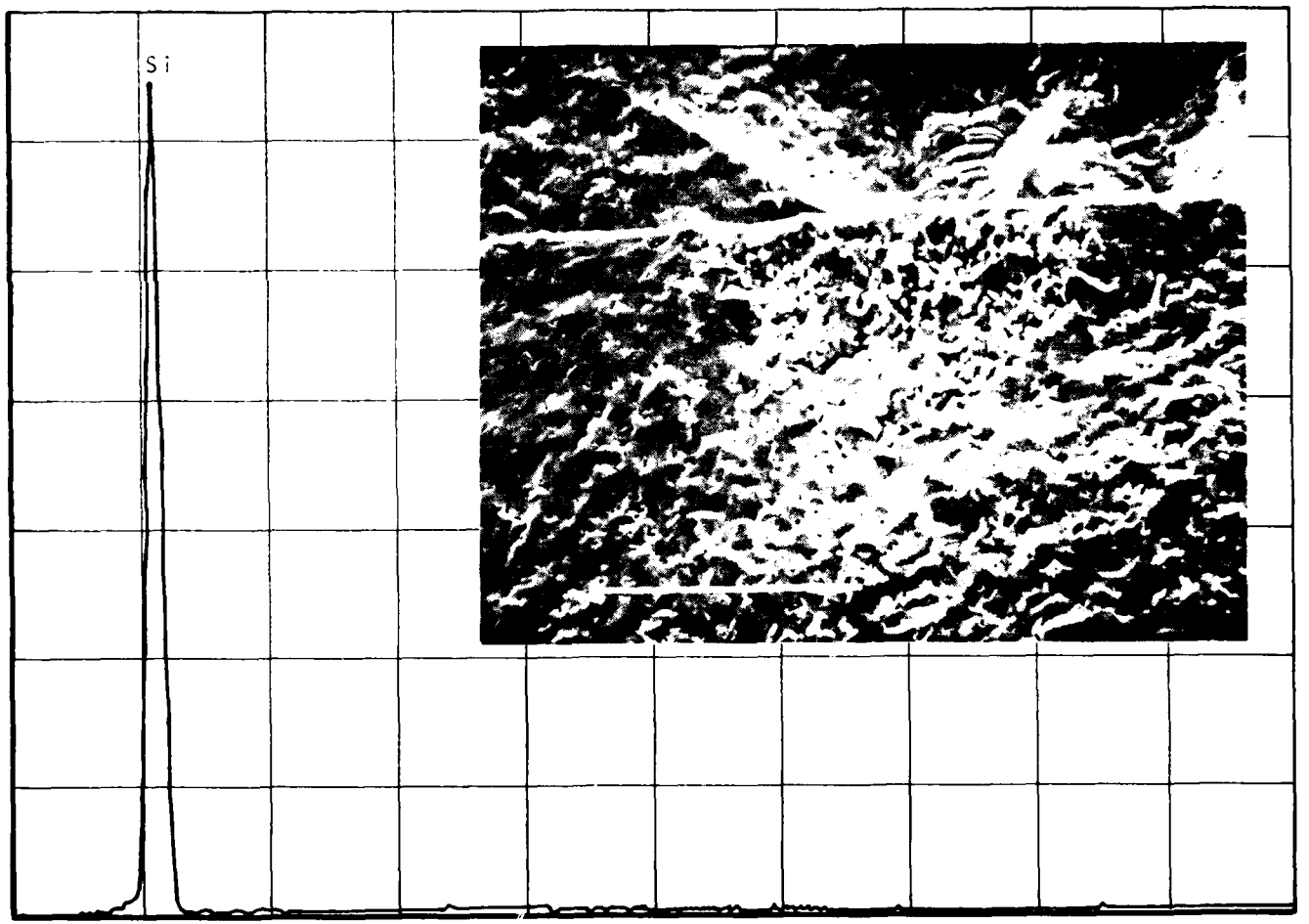

F-31356

Figure 4-6. X-Ray Spectrum at the Point of Intergranular Fracture and SEM Micrograph for Sample 107, Group 106 (350X)

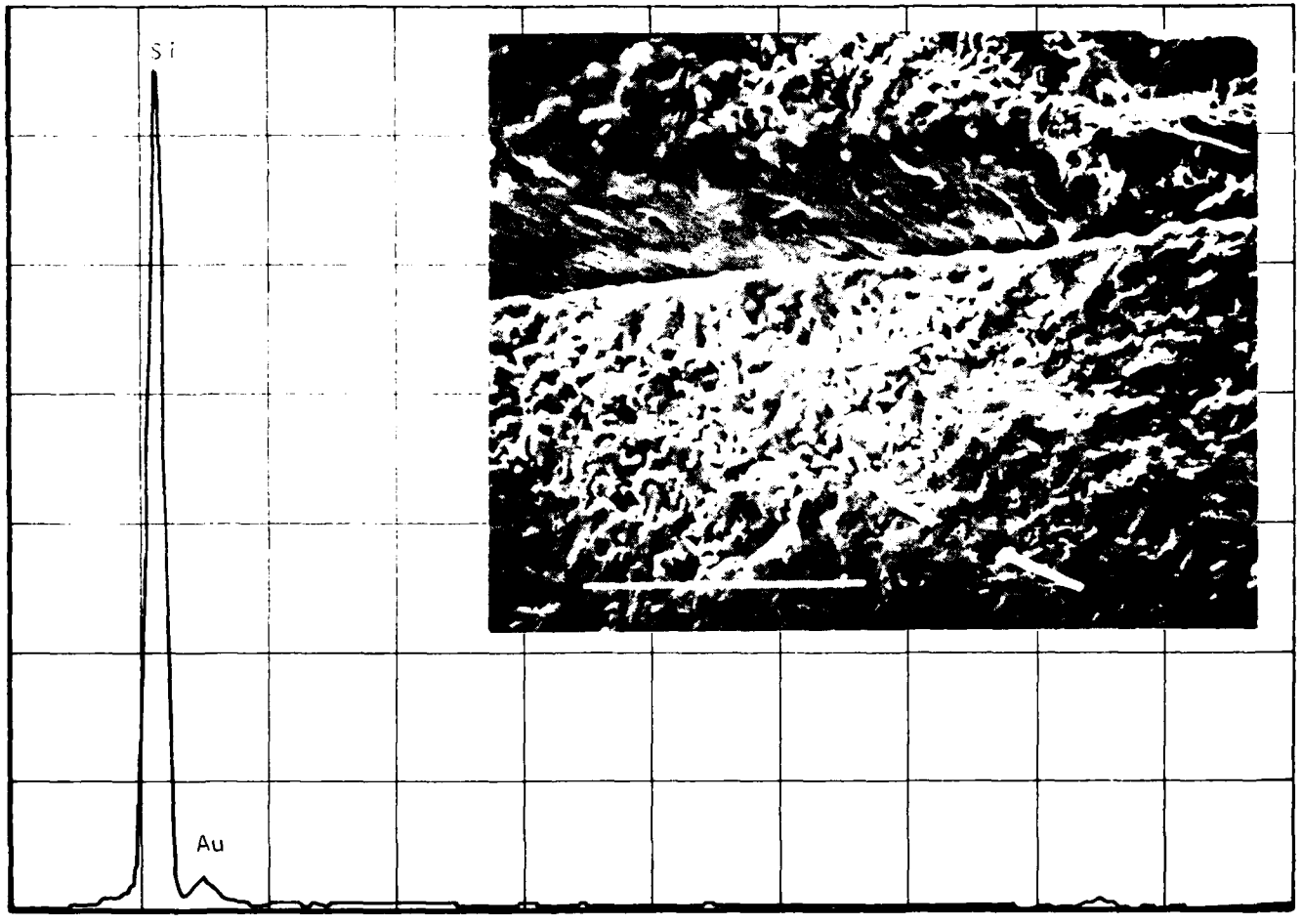

Figure 4-7. X-Ray Spectrum at the Point of Intergranular Fracture and SEM Micrograph for Sample 102, Group 118 (350X)

SECTION 5

DISCUSSION

The results of this experimental investigation indicate that the processing of SASC should be improved to eliminate the flaws causing failure near the as-fired and as-formed surface. These flaws appear to be the result of material preparation. Although the size distribution and type of flaws varied between the samples from the two programs, there appears to be no large difference in the mechanical strength variation with strain rate and temperature (see Figure 5-1).

A smaller percentage of failed specimens were in a condition that would allow examination by SEM for the ONR-2 program (see Table 4-3). This was due to the generally smaller-sized critical flaws that caused high-energy fractures. In such cases, the failures are nearly explosive due to the rapid release of stored elastic strain energy. The large number of small pieces makes it difficult to identify the fracture origin. In support of this observation, a larger percentage of ONR-2 specimens (89.2 to 79.5) failed from flaws on the tensile surface of the specimens.

Although the powder preparation and high-temperature processing were performed at Carborundum under proprietary conditions, the following discussion is offered as a possible explanation for the type, size, and variation of flaws found in this investigation. The size and shape of the types of flaws causing failure in both programs was quite different, which indicates that the material processing parameters for each set of test specimens may have been varied. Generally, the flaws found in the ONR-3 program were larger and were associated with voids, internal-subsurface cracks, and areas that appear to be not fully sintered (low density). The ONR-2 flaws were primarily low-density areas and pores. A very small percentage of failures was associated with subsurface cracks. Most of these flaw types might be expected from the cold pressing of powders, which was the processing technique used to fabricate all the samples.

The cold powder pressing technique can lead to areas near the pressing die surface that are not well compacted. Also, die lubricants or binder agents may be forced into the near-surface layers of the compacted body. Agglomerated freeze-dried or spray-dried powders form shell-like spheres that can remain rigid during the compaction process, yielding preformed voids. Another common defect is subsurface cracks that form when a nonuniform density sets up stress gradients in the relatively weak compacted body. These stresses can be relieved by cracking of the body. Similar cracks also are observed when the die pressure is removed too quickly from the shape being pressed.

During the ONR-2 program it was believed that sintering agents used in the processing of SASC may have played an important part in the material degradation under oxidizing and salted environments at high temperatures. Their role in the fracture or crack growth process is still not clear. Attempts to examine the strength-limiting defects for concentrations of any foreign materials proved negative. Concentrations, if any, were probably below the detectability of the SEM.

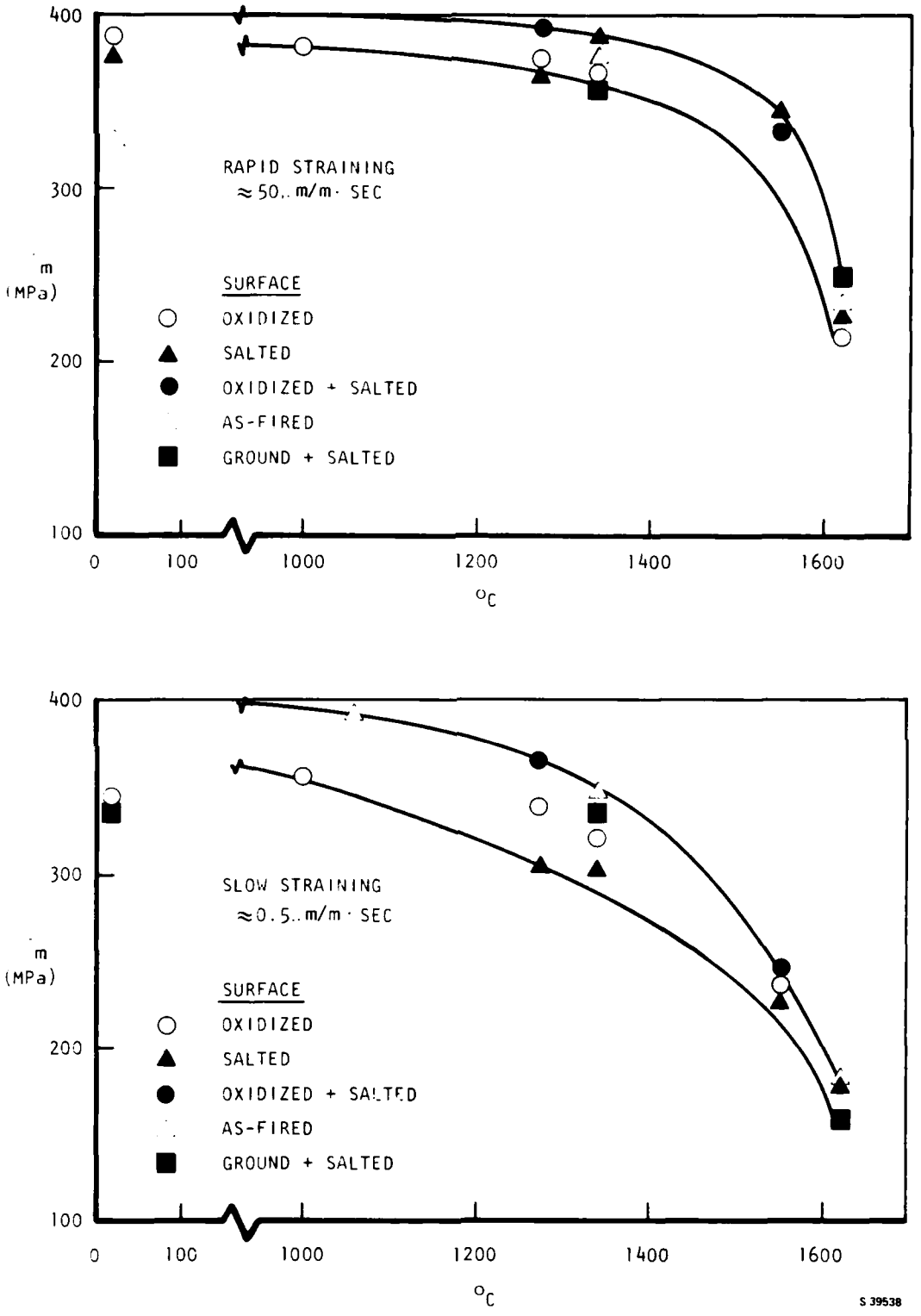

Figure 5-1. Failure Stress Versus Temperature at Two Strain Rates for SASC As-Fired Surfaces

Examples of the variation found for each type of flaw are presented in detail for both ONR-2 and ONR-3. These micrographs can be used as a guide for comparison of samples from each program and with other programs.

The variation in size and shape of pits and pores found as failure origins in ONR-2 is shown in Figure 5-2. All micrographs are at 350X and generally show both halves of the fracture surface. Micrographs 5-2a through 5-2f show pits open to the tensile surface. Micrographs 5-2a through 5-2d show pits on the as-fired tensile surface and 5-2e and 5-2f show pits exposed by surface finishing of the ground surface. Micrographs 5-2a through 5-2e show rounded surfaces within the pit probably due to the high-temperature exposure of these surfaces during oxidation or salt coating. The pit surfaces in micrograph 5-2f are angular by comparison. Micrographs 5-2g through 5-2L show pores closed to the specimen surface. These defects show a great variation in size and shape. Micrographs 5-2k and 5-2L show the two largest pores found. Both pores seem to be surrounded by low-density material and most of the grains on the pore walls are well rounded. It is believed that such pores are the result of large uncrushed powder agglomerates during the cold power pressing when the material was processed.

Low-density areas that were the failure origins in some ONR-2 specimens are shown in Figure 5-3. When some of this porous region is linked together it forms a flaw large enough to cause failure. Low-density areas were found as fracture origins in samples tested at both high temperature (5-3a through 5-3c) and room temperature (5-3d). It can be speculated that the origin of the low-density areas is the incomplete powder compaction in local areas during the cold powder pressing operation.

Micrographs of the flake-like cracks or voids found in the ONR-2 samples are shown in Figure 5-4. Relatively few flake-like cracks were found in ONR-2 and they are not found in a group as they are in ONR-3 specimens. The crack walls appear to be covered with rounded grains similar to the appearance of the pits and voids in Figure 5-2.

Inclusions found on the fracture surfaces of specimens are shown in Figure 5-5. These inclusions do not appear to have any difference in composition from the surrounding matrix, at least at the detectability of the SEM X-ray analysis. The texture of the inclusions was of two types as shown in micrographs 5-5a and 5-5b. In micrograph 5-5a the inclusion had a grainy, angular appearance and in micrograph 5-5b the inclusion is a densified mass within a slightly larger hole. The nature of these defects is unknown.

Unusually large surface grains that were the cause of failure are shown in Figure 5-6. It is well known that the strength of ceramic materials decreases with increasing grain size, so it is not surprising that several large grains would be the fracture origin on the tensile surface. The sharp angles between these large grains may have enhanced the stress concentation at this particular point.

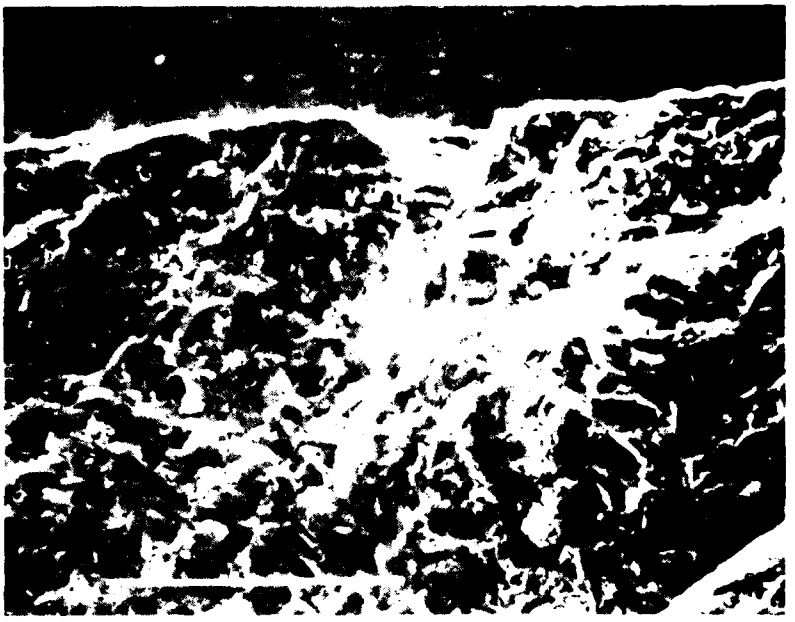

a. GROUP 2, SAMPLE 4, 350X

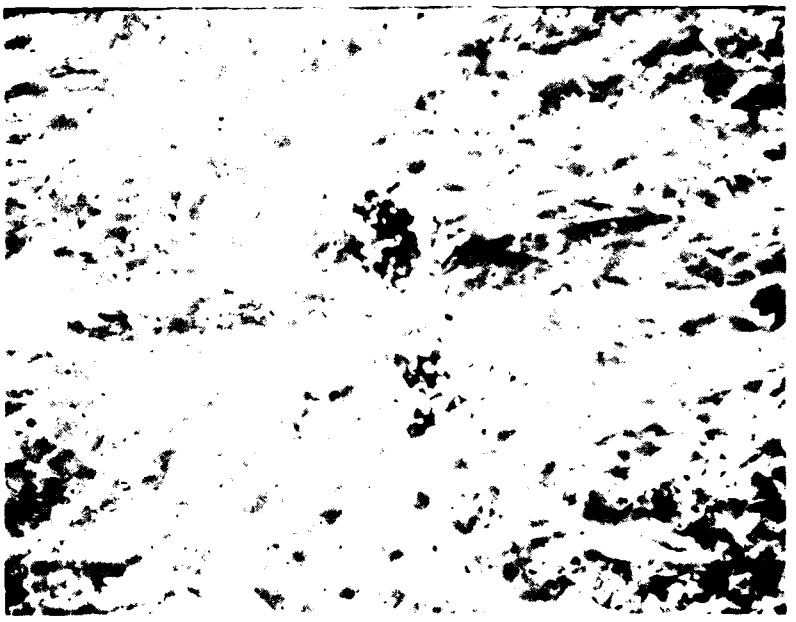

F-31322

b. GROUP 2, SAMPLE 1, 350X

Figure 5-2. Pit and Pore Failure Origins in CNR-2 Samples

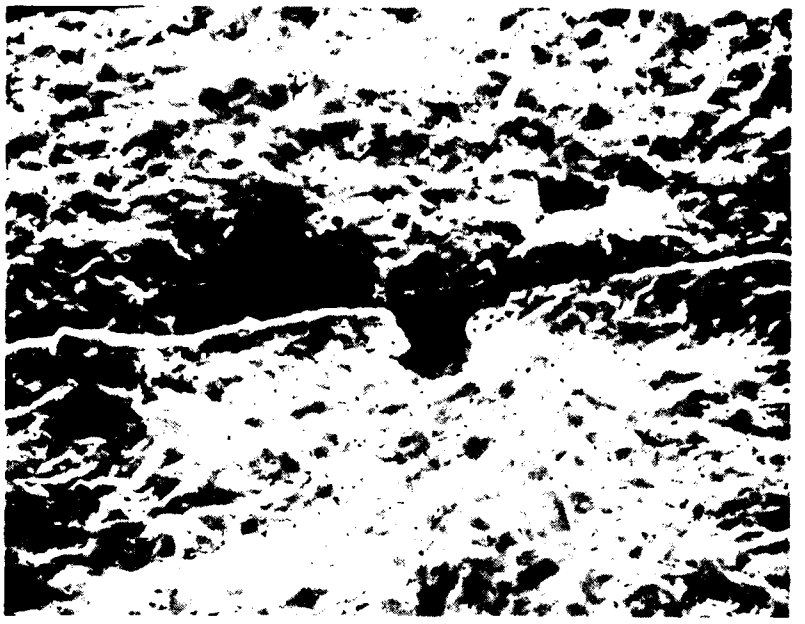

c. GROUP 2, SAMPLE 3, 350X

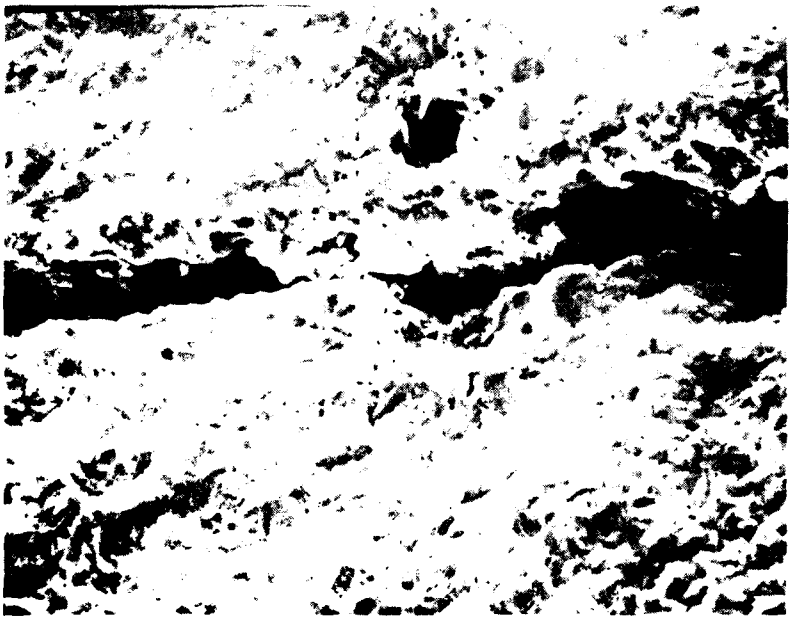

F-31323

d. GROUP 11, SAMPLE 5, 350X

Figure 5-2. (Continued)

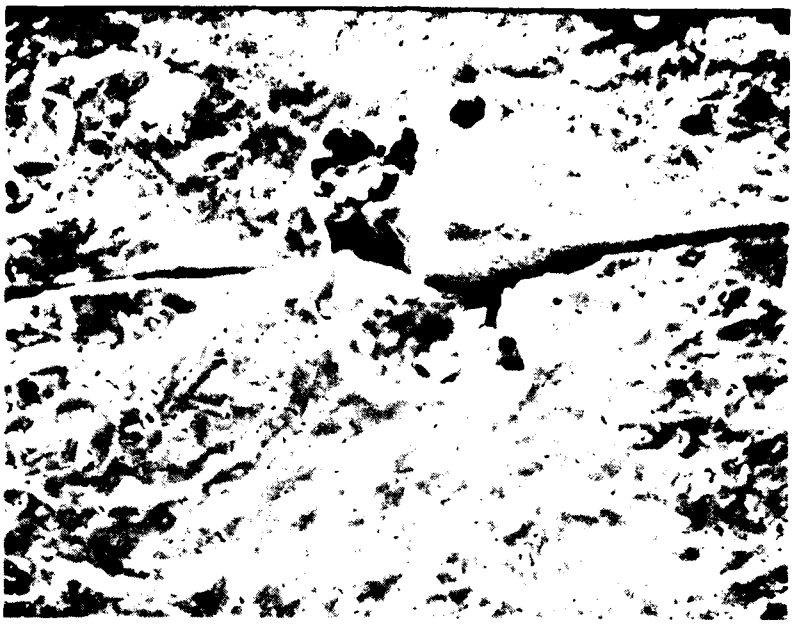

e. GROUP 20, SAMPLE 3, 350X

F-31324

f. GROUP 19, SAMPLE 7, 350X

Figure 5-2. (Continued)

q. GROUP 12, SAMPLE 4, 350X

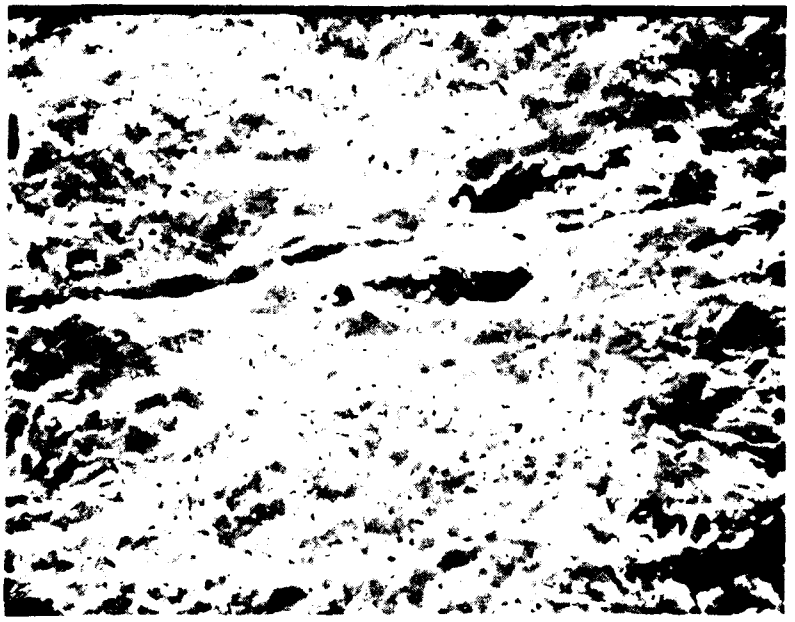

F-31325

r. GROUP 12, SAMPLE 5, 350X

Figure 5-2. (Continued)

i. GROUP 1, SAMPLE 5, 350X

F-31326

i. GROUP 13, SAMPLE 2, 350X

Figure 5-2. (Continued)

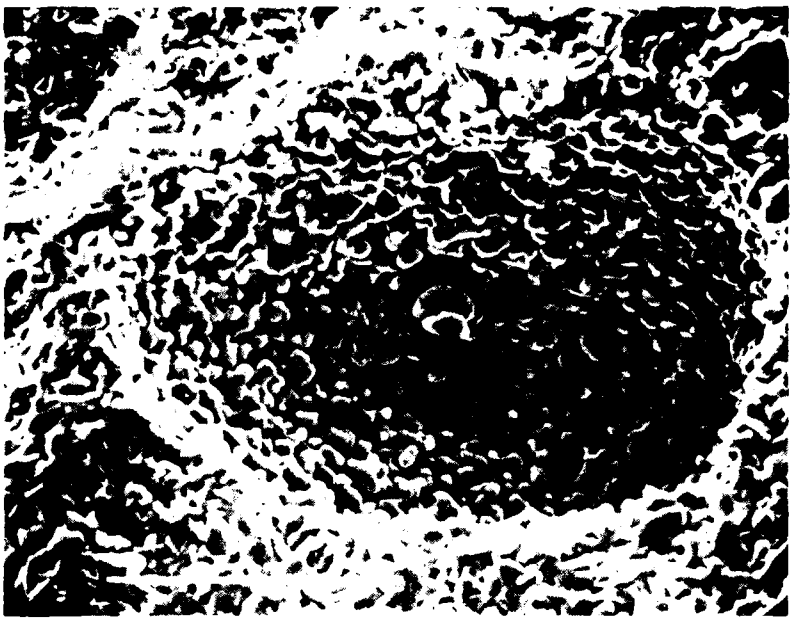

k. GROUP 2, SAMPLE 5, 350X

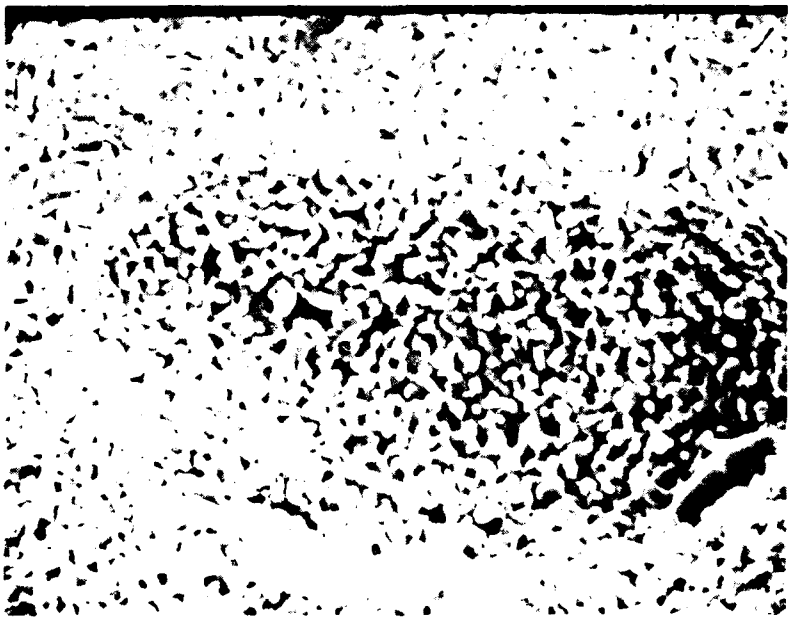

F-31327

l. GROUP 23, SAMPLE 2, 350X

Figure 5-2. (Continued)

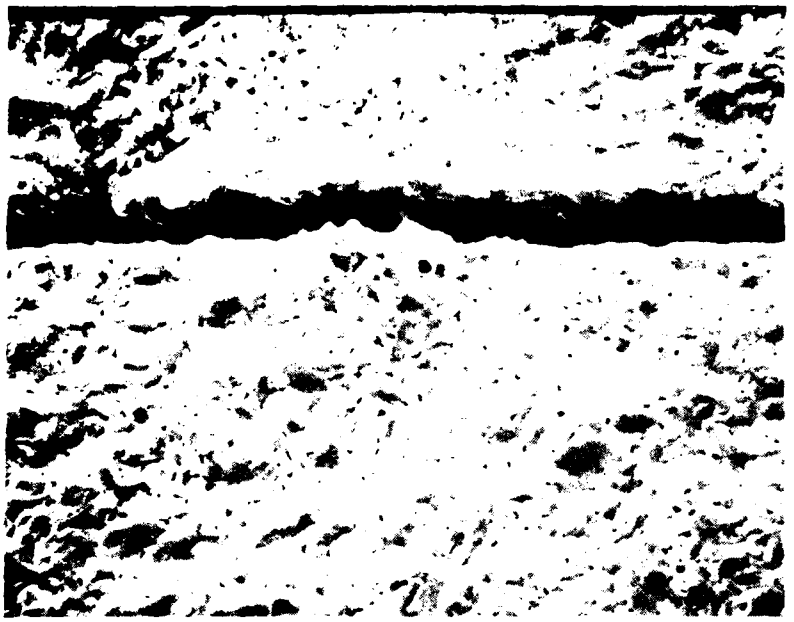

a. GROUP 15, SAMPLE 2, 350X

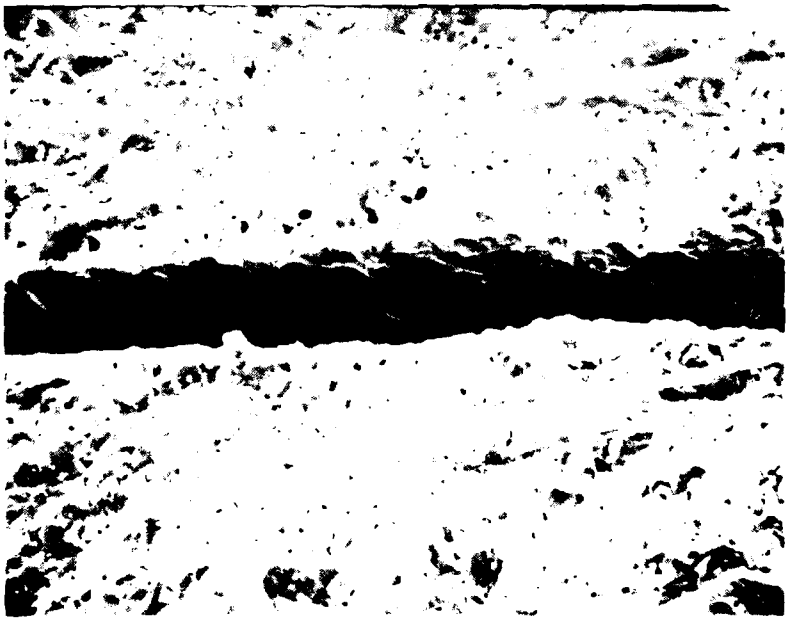

F-31328

b. GROUP 15, SAMPLE 1, 350X

Figure 5-3. Low-Porosity Failure Origins in CNP-2 Samples

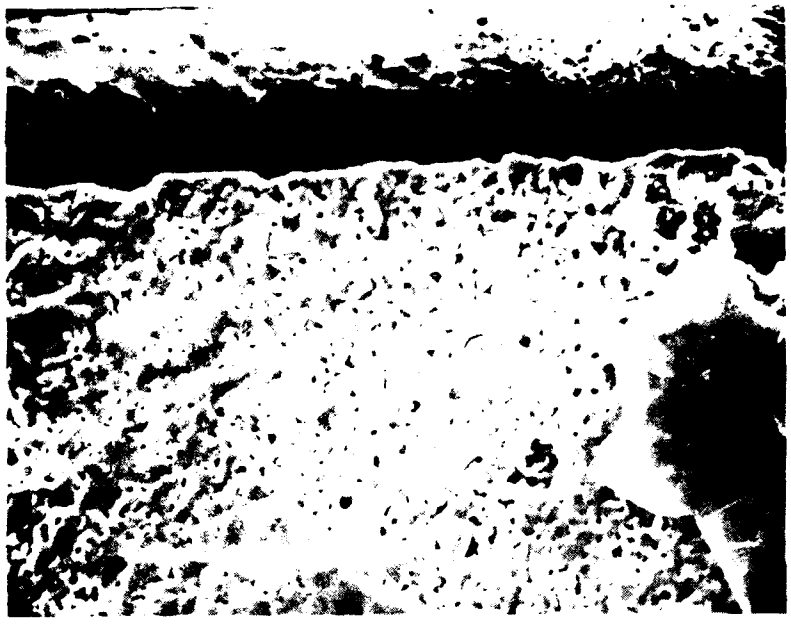

c. GROUP 10, SAMPLE 1, 350X

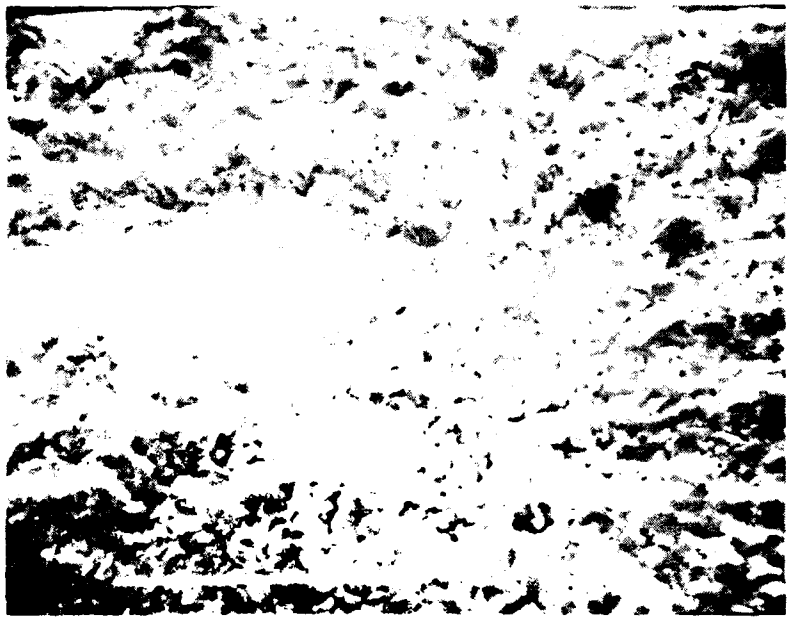

F-31329

d. GROUP 1, SAMPLE 7, 350X

Figure 5-5. (Continued)

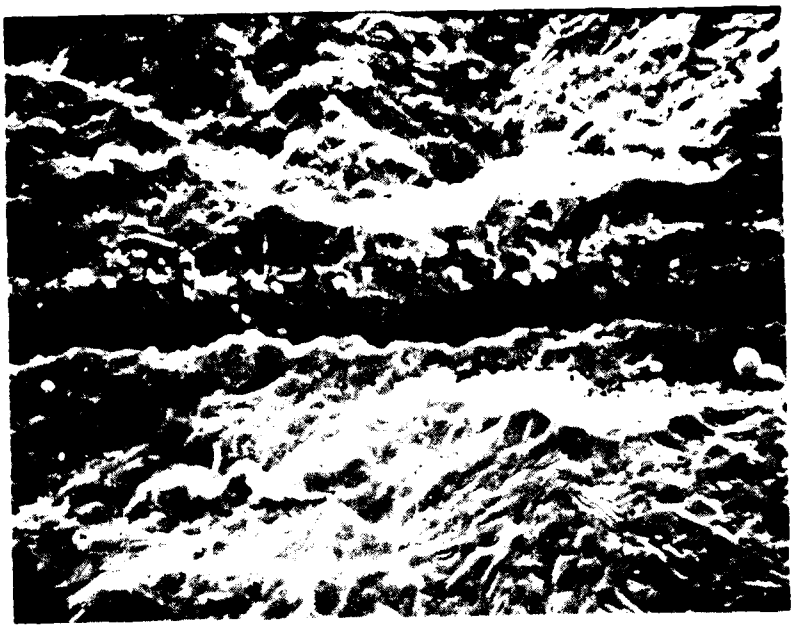

a. GROUP 17, SAMPLE 1, 350X

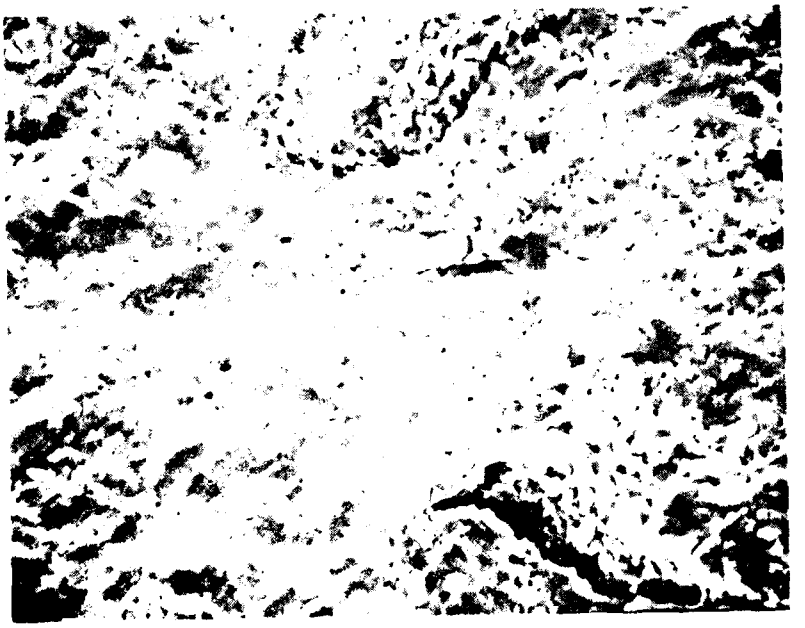

F-31330

b. GROUP 9, SAMPLE 3, 350X

Figure [illegible] Fracture Surfaces

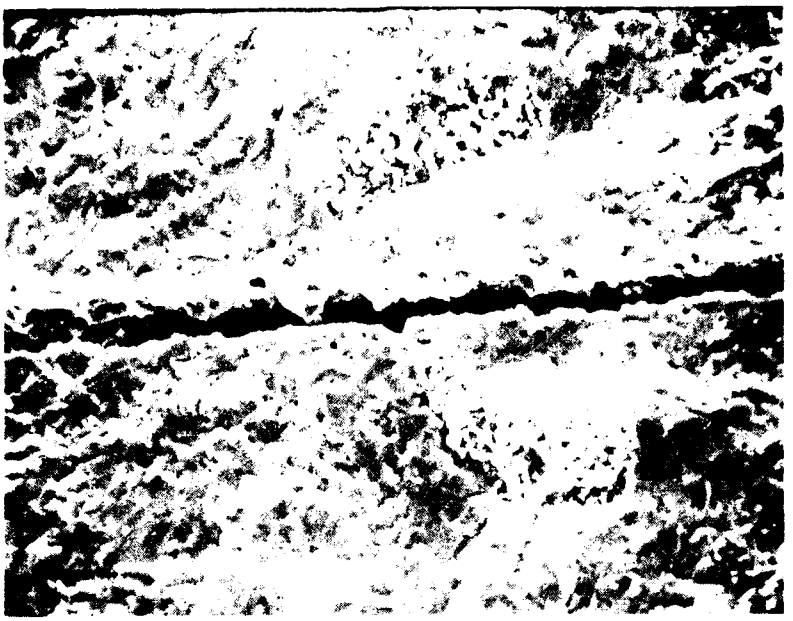

GROUP 23, SAMPLE 1, 350X

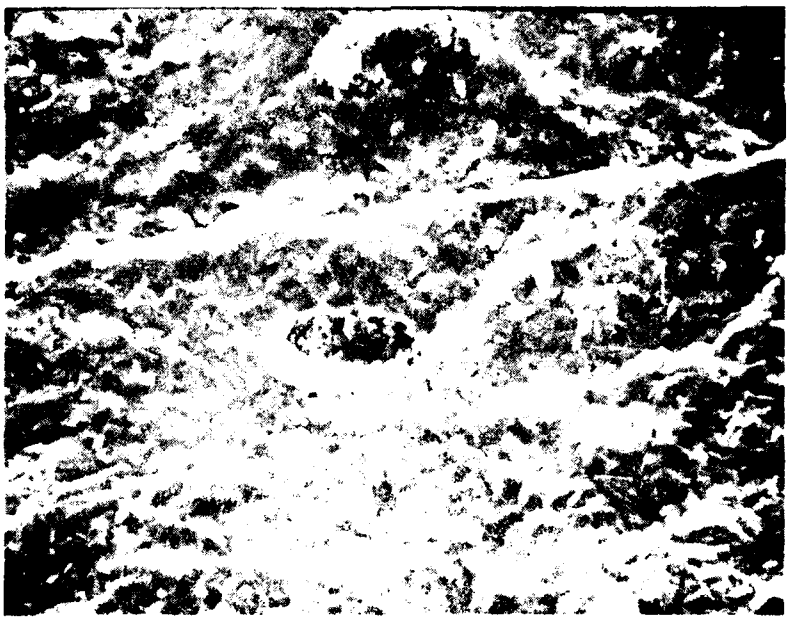

F-31331

GROUP 22, SAMPLE 1, 350X

Figure 5-[illegible] Surface

F-31332

Figure 5-6. Large Surface Grains at the Fracture Origin of an ONR-2 Specimen for Sample 2, Group 3 (350X)

Intergranular fracture near the origin of specimens tested at 1620°C is shown in Figure 5-7. Micrographs 5-7d, f, and g are at 150X. The regions of intergranular fracture are characterized by the bumpy irregular fracture surfaces where a large percentage of whole grains can be seen. This area is associated with slow crack growth. Adjacent to this area a relative flat transgranular fracture area can be seen. This area is associated with fast fracture. In some micrographs, the defect that caused a stress concentration is visible (5-7a is a void, 5-7b is a surface pit). Many of these defects may have been covered up by the heavy formation of oxide after this very high-temperature test, as in micrographs 5-7c and 5-7f.

The defects that caused failure of specimens in the ONR-3 program were similar to those found in the ONR-2 program. Some exceptions were the frequent occurrence of flake-like pores and generally larger flaws.

Some typical pores found as the critical defect on the fracture surface are shown in Figure 5-8. Micrographs 5-8a and 5-8b show typical pits found on the surface of tensile surfaces. Micrographs 5-8c through 5-8g show pores in the bulk of the material near the tensile surface that were the strength limiting defects. Most of these pores do not have clearly-defined walls. Most of the larger pores are associated with low-density regions.

One of the most common defects was the flake-like crack that ran parallel with the tensile-stressed face. The typical flake-like defects are shown in Figure 5-9. Micrograph 5-9i is at 250X. All of the flake-like cracks that were found as fracture origins were very close to the tensile surface. Micrographs 5-9d, e, g, h, and i show flake-like defects partially open to the tensile-stressed surface. Some of these defects appear to be associated with low-density regions. The defects are found at nearly all the conditions tested. It is believed that these defects resulted from the local insufficient compaction of powder during the cold powder pressing before sintering.

The defects found to be inclusions are shown in Figure 5-10. These inclusions are similar in size, shape, and appearance to those found in the ONR-2 specimens. Also, these defects do not show any detectable difference in composition from the matrix at the detectability limit of the SEM X-ray analysis. Most of these inclusions were found on the fracture surfaces of specimens tested at room temeprature (micrographs 5-10b through 5-10e). Only one inclusion was found at high-temperature (micrograph 5-10a). Since these defects apparently do not have any chemical difference from the matrix, it is possible that these areas were originally low-density areas where most of the material in the vacinity sintered into a small dense compact surrounded by a shell-like void.

A relatively few specimens failed from regions of low-density in the ONR-3 specimens, but many had low-density associated with a particular type of defect (Figure 5-11). Micrograph 5-11a shows a low-density area associated with a flake-like crack. Micrographs 5-11b and 5-11c show low-density areas surrounding pores in the SASC.

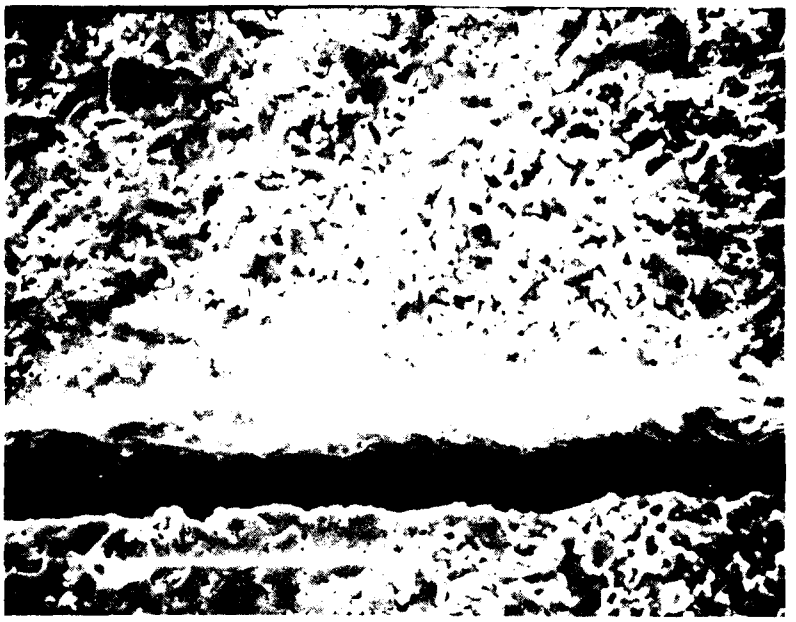

a. GROUP 16, SAMPLE 1, 350X

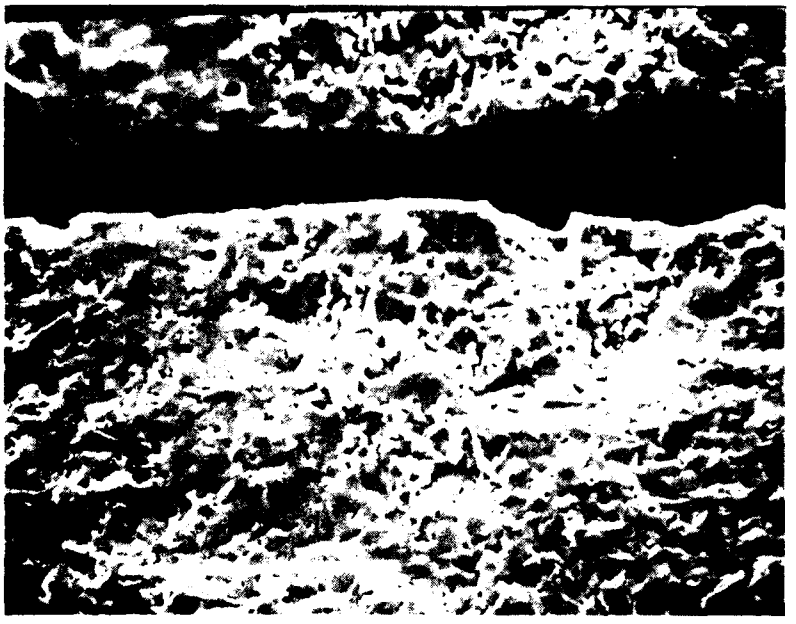

F-31333

b. GROUP 16, SAMPLE 3, 350X

Figure 5-7. Intergranular Fracture at 1620°C for ONR-2 Specimens

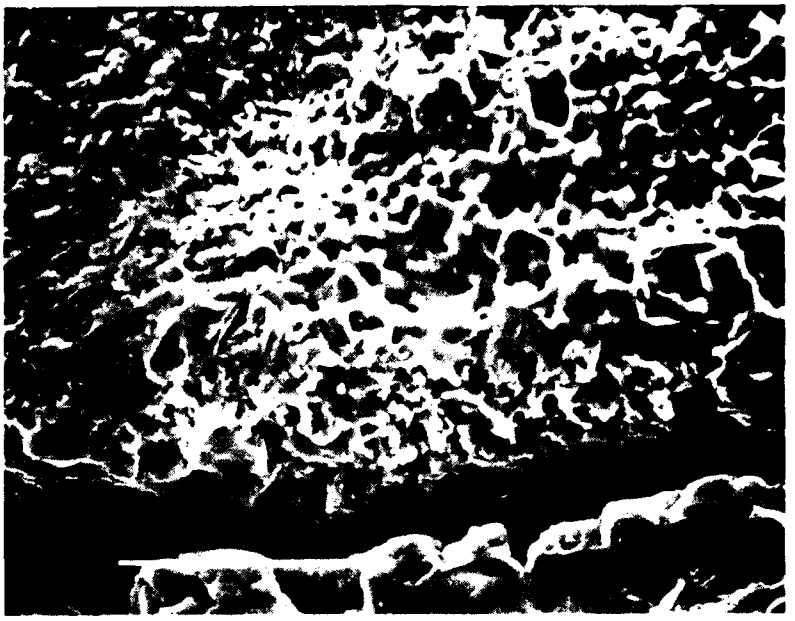

c. GROUP 16, SAMPLE 6, 350X

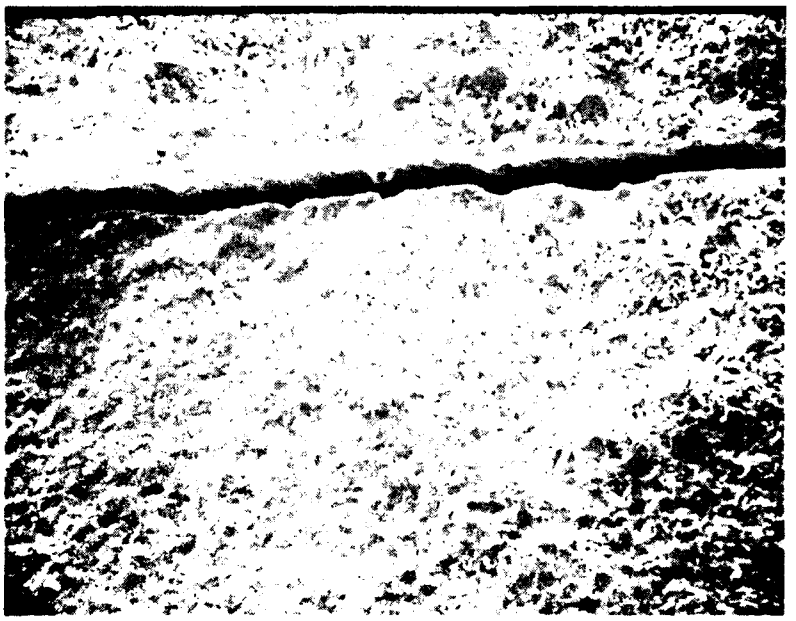

F-31334

d. GROUP 17, SAMPLE 3, 150X

Figure 5-2. (Continued)

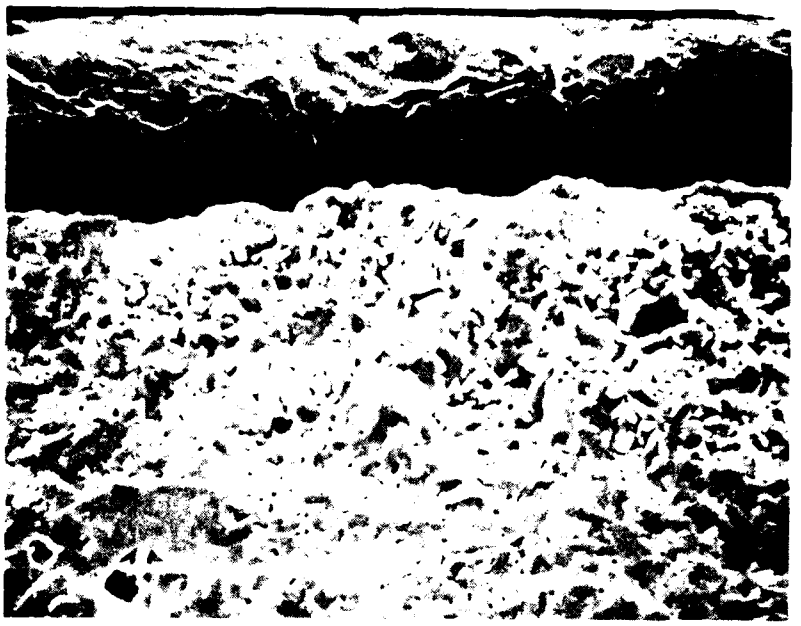

e. GROUP 17, SAMPLE 4, 350X

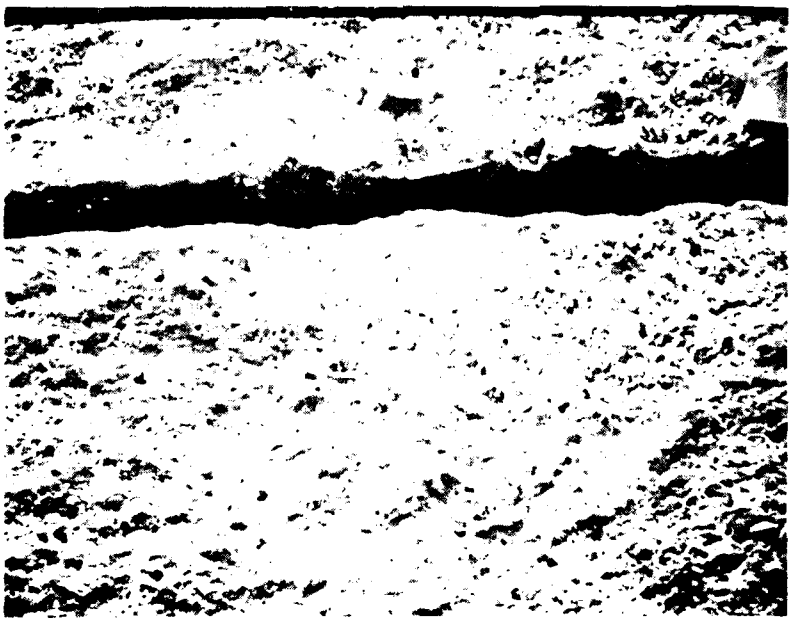

F-31335

f. GROUP 18, SAMPLE 2, 150X

Figure 5-7. (Continued)

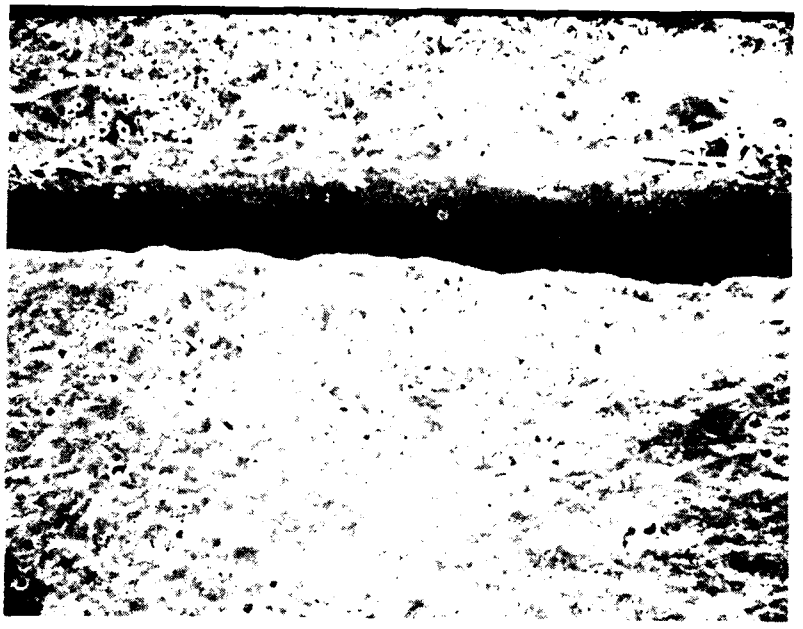

F-31336

g. GROUP 18, SAMPLE 4, 150X

Figure 5-7. (Continued)

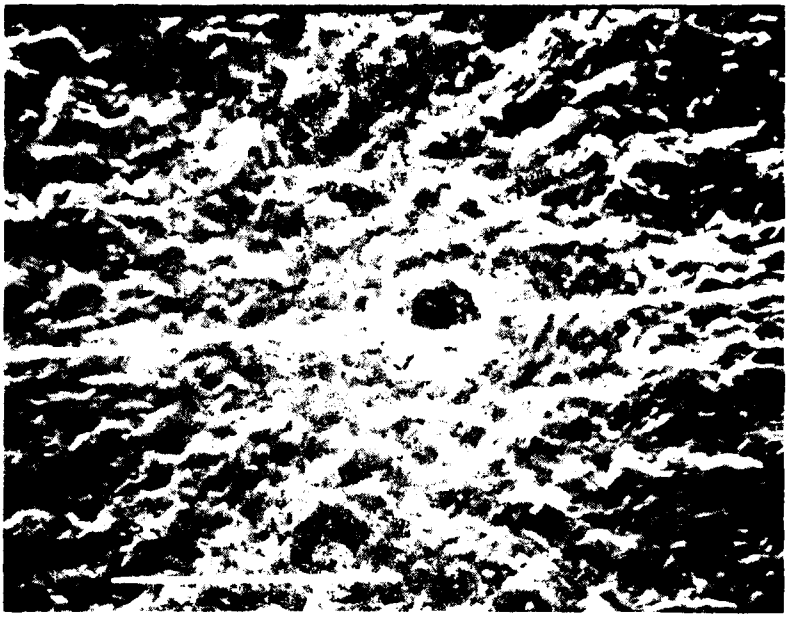

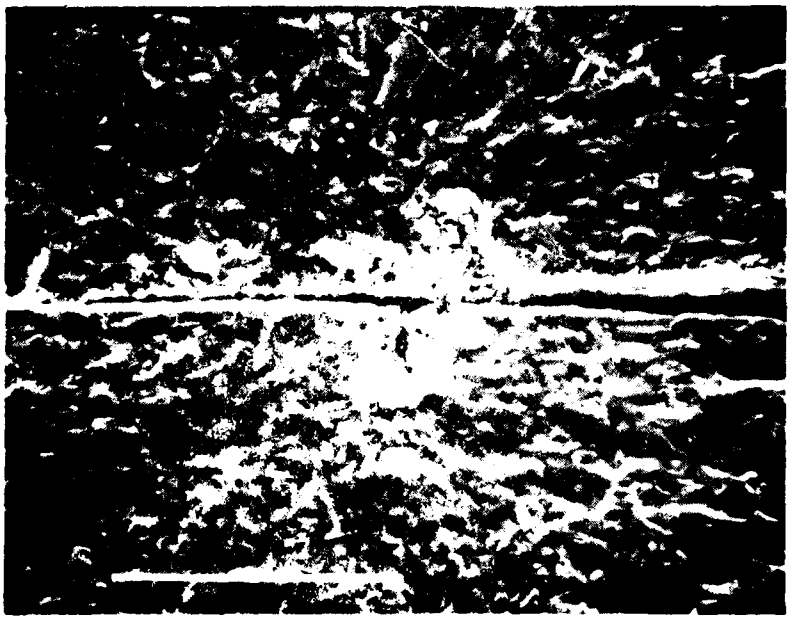

F-31337

c. GROUP 101, SAMPLE 194, 350X

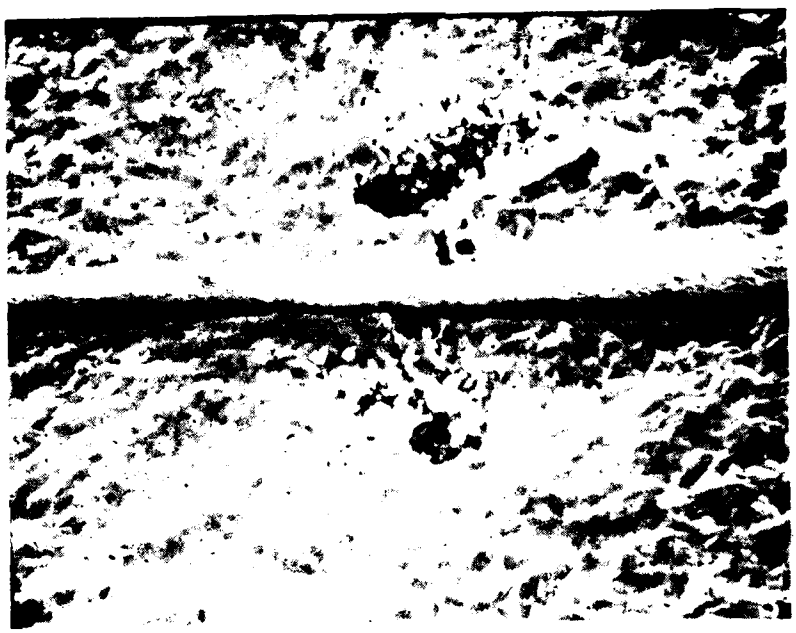

F-31338

d. GROUP 108, SAMPLE 90, 350X

Figure 5-1. (Continued)

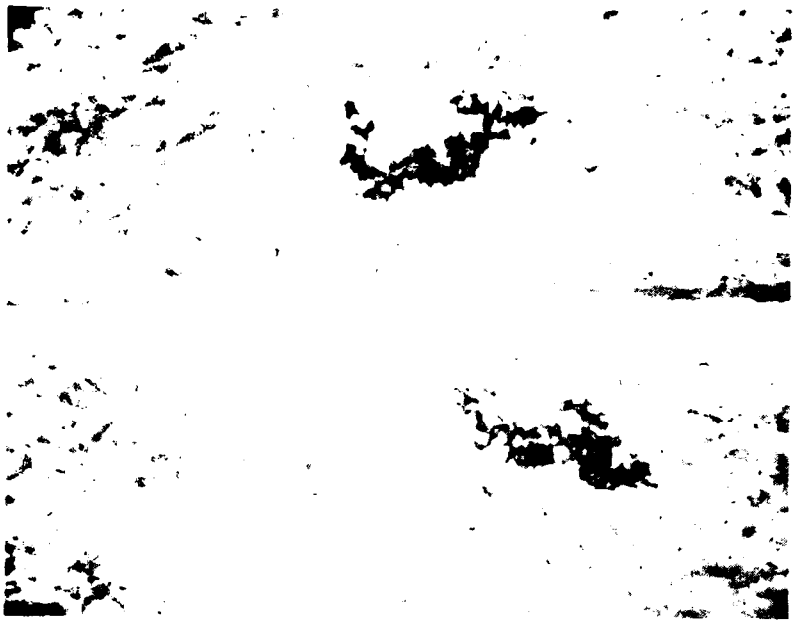

H. GROUP 119, SAMPLE 5, 350X

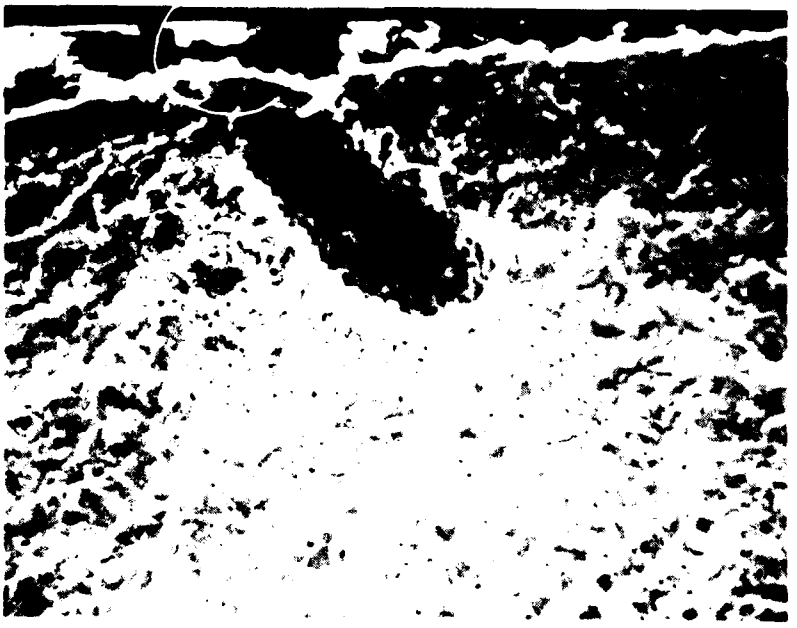

F-31339

I. GROUP 115, SAMPLE 7, 350X

Figure 5-8. (Continued)

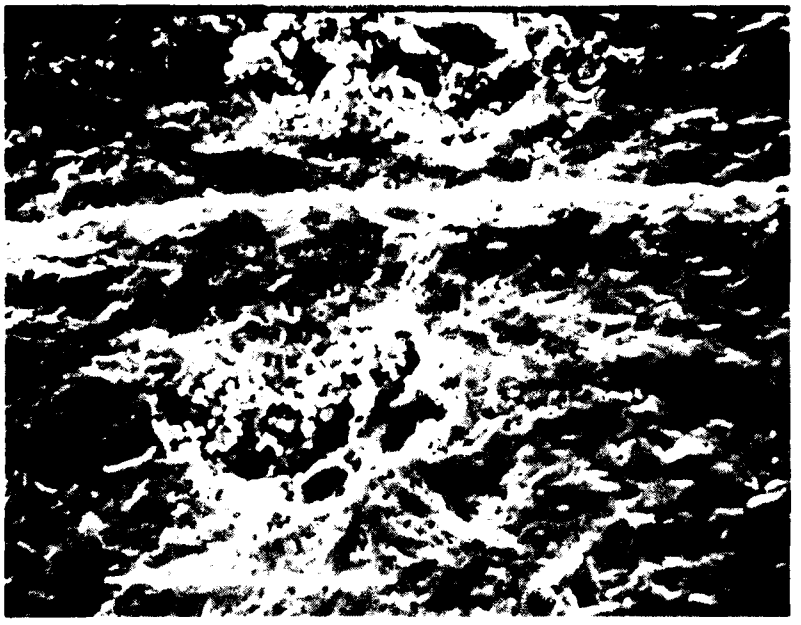

F 31340

GROUP 100, SAMPLE 183, 350X

Figure 5-5. (Continued)

GROUP 115, SAMPLE 18, 350X

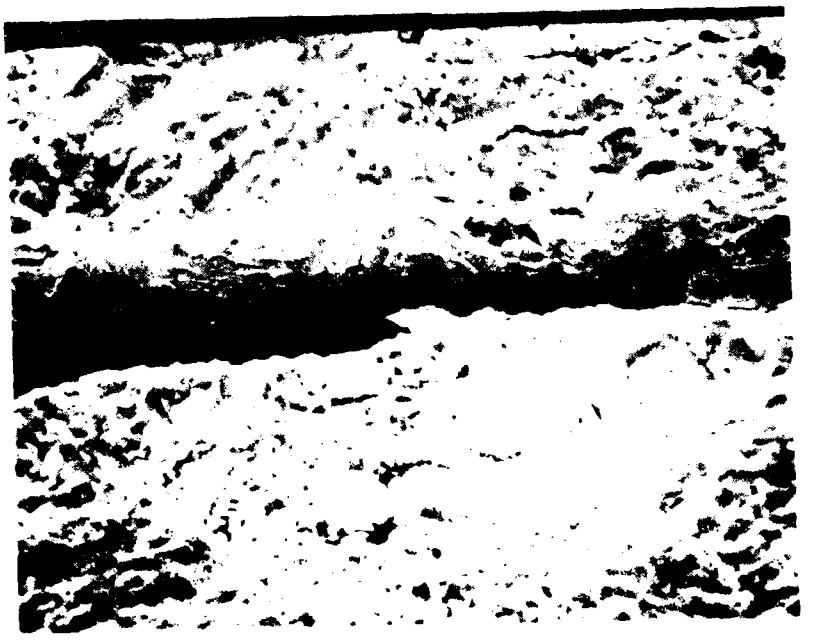

F 31341

GROUP 114, SAMPLE 159, 250X

Figure [illegible]

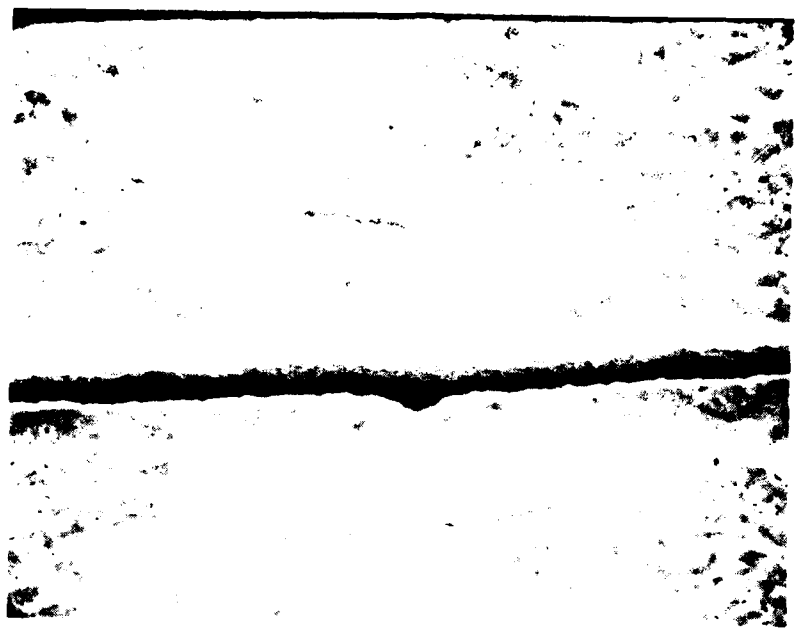

c. GROUP 109, SAMPLE 190, 350X

F 31342

d. GROUP 108, SAMPLE [illegible]X

[illegible]

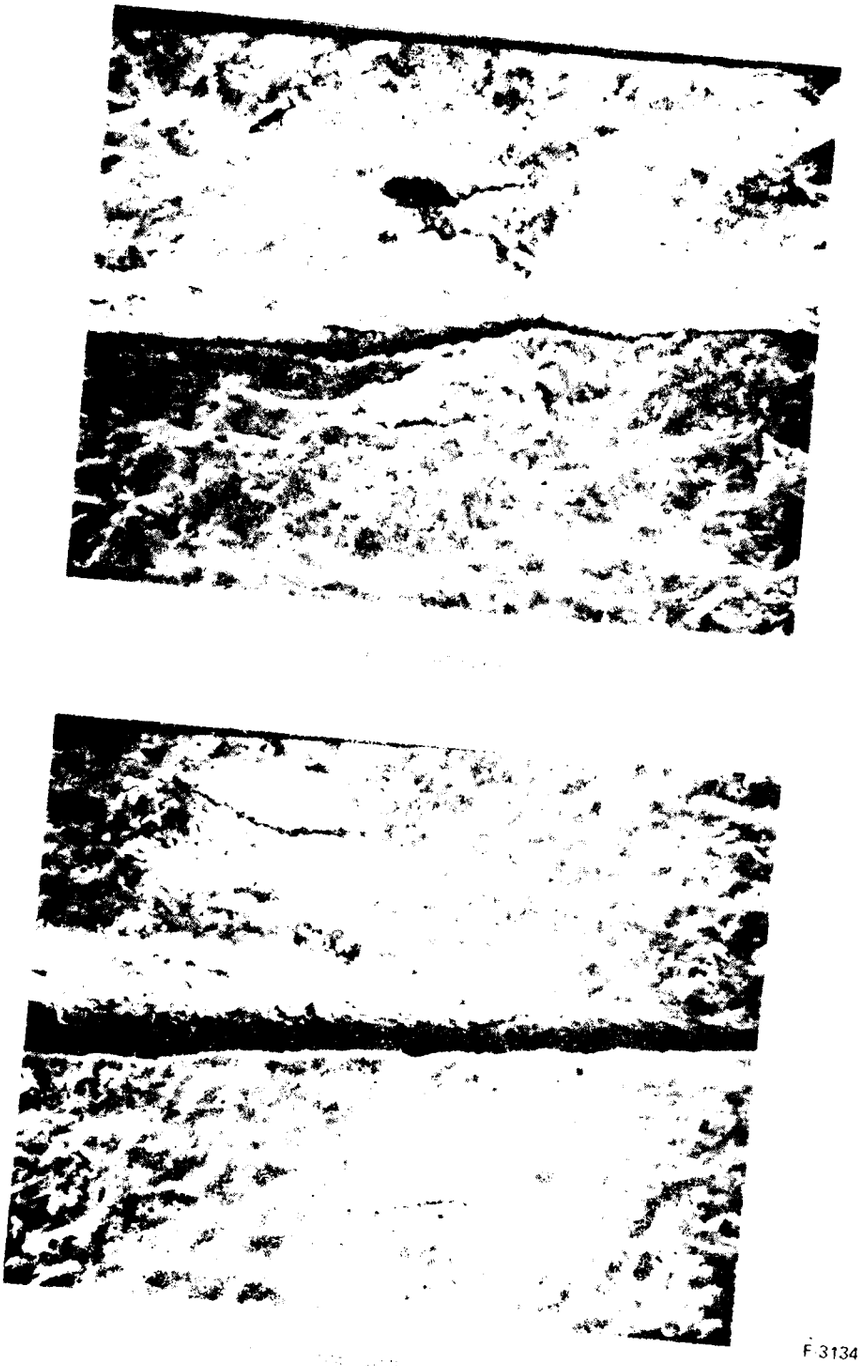

F 31343

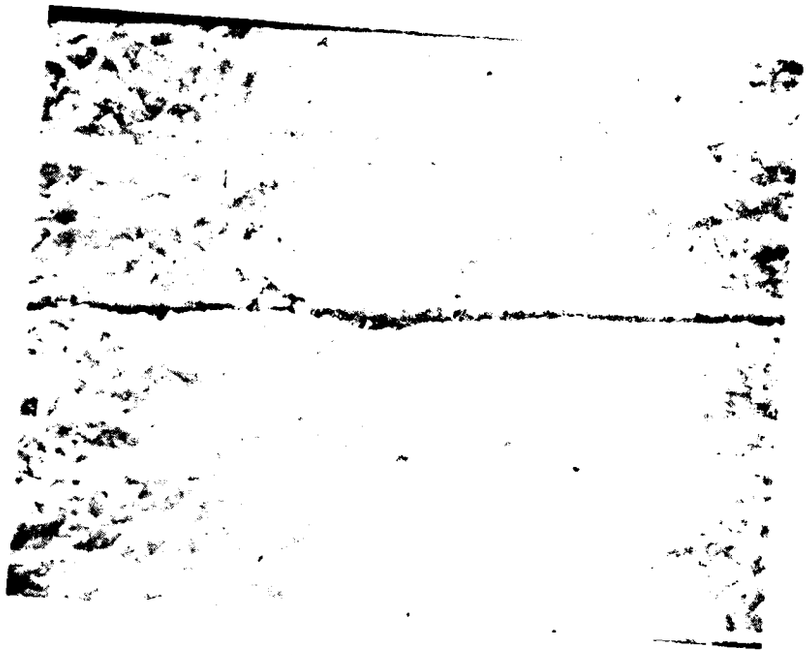

F 31344

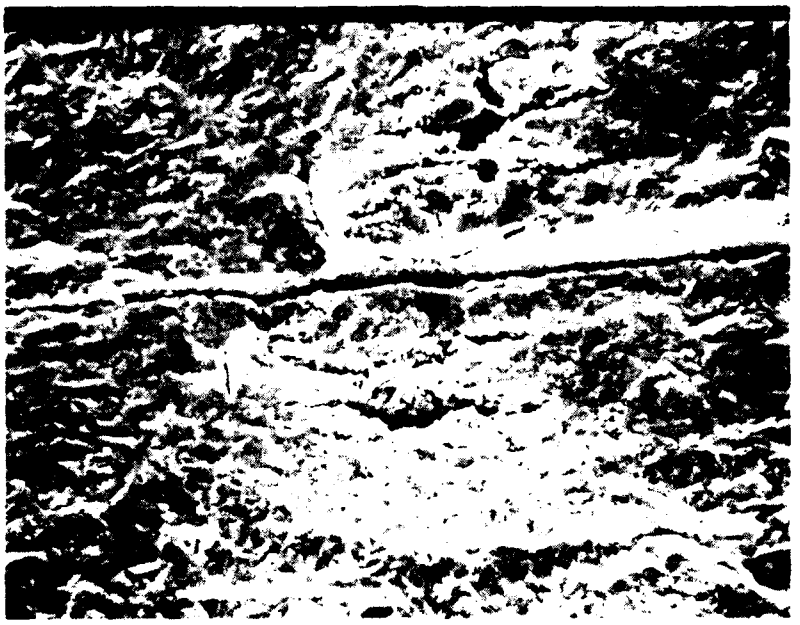

F-31345

GROUP 110, SAMPLE 2, 250X

Figure 5-5. (Continued)

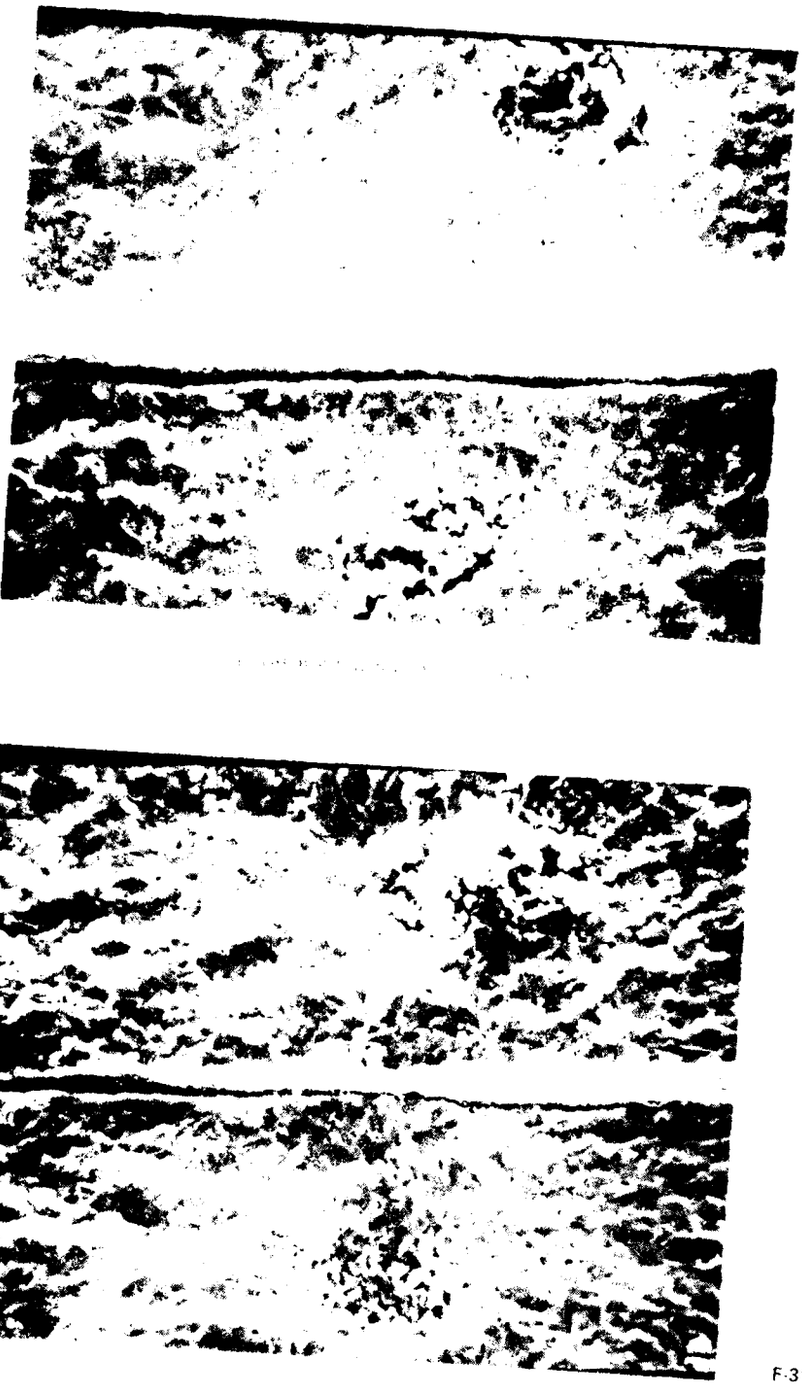

F-31346

imens

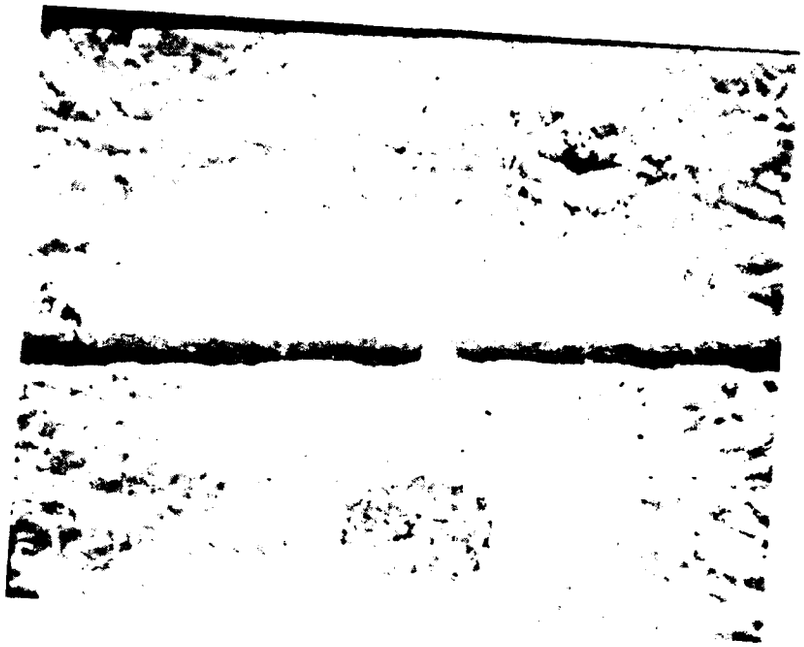

c. GROUP 101, SAMPLE 13Z, 350X

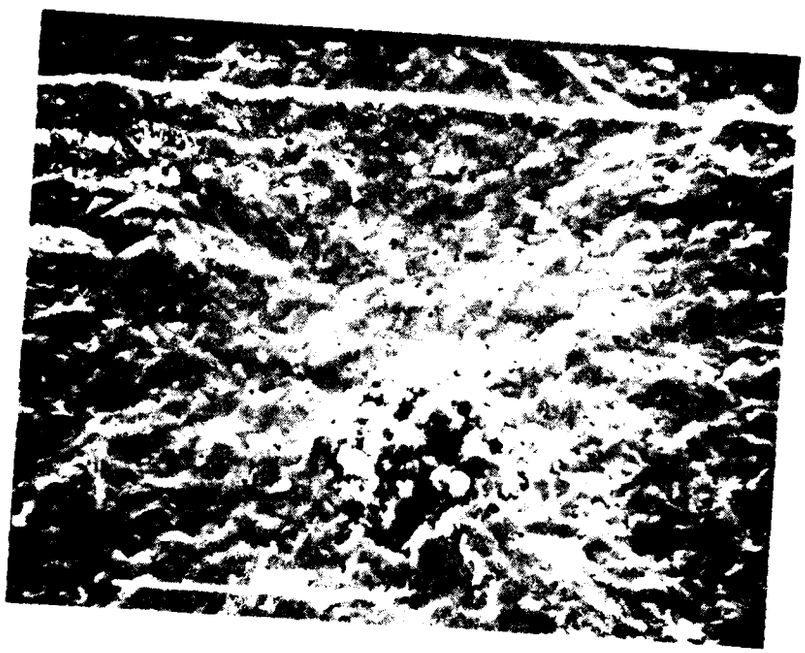

F-31347

d. GROUP 101, SAMPLE 13, 350X

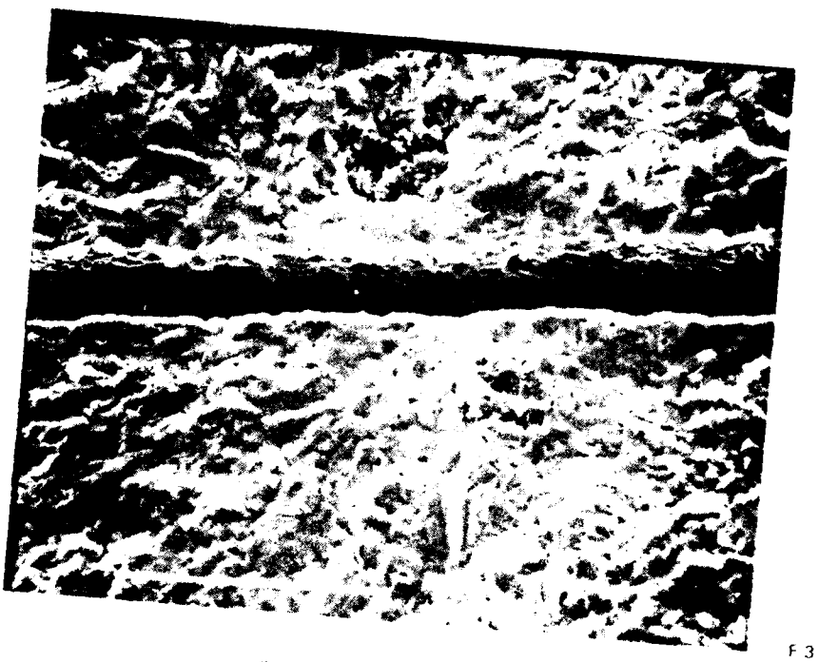

F 31348

GROUP 113, SAMPLE 49, 350X

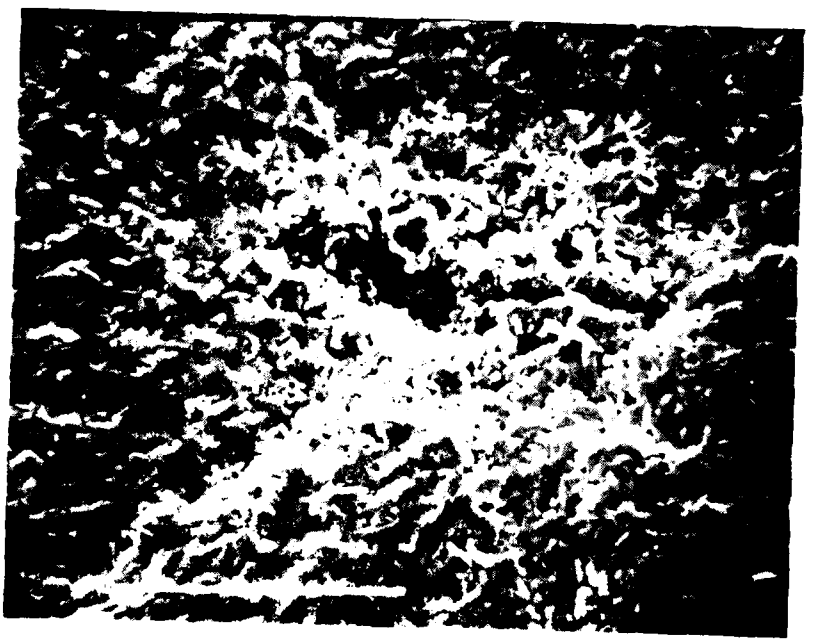

F-31349

GROUP 101, SAMPLE 26, 350X

Figure [illegible] Regions

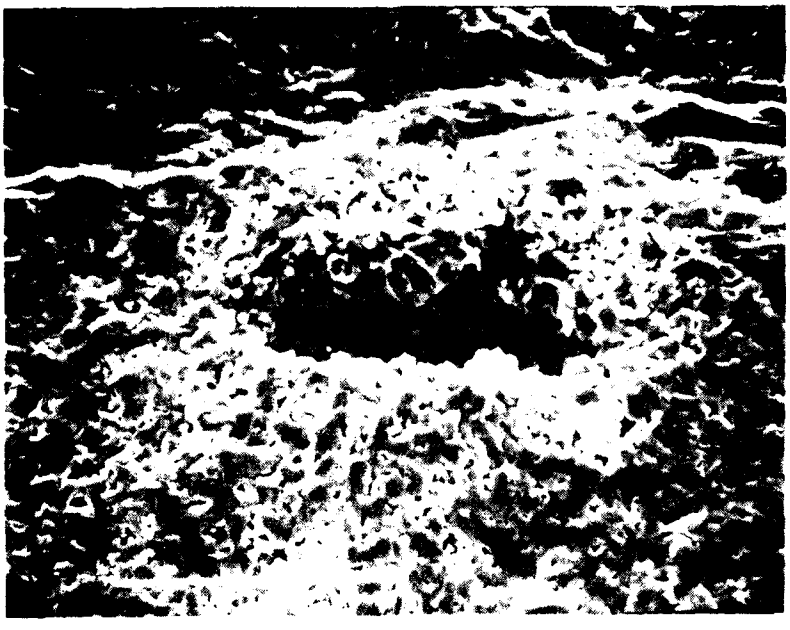

F-31350

GROUP 104, SAMPLE 46, 350X

Evidence of slow crack growth by intergranular fracture was observed at 1550°C (Figure 5-12). Micrographs 5-12a through 5-12c are from samples tested after oxidation, and micrograph 5-12d is from a salt-treated specimen. Evidence of SCG was found on specimens from the oxidized and salt-treated groups tested at 1550°C, but it was difficult to obtain good micrographs of the fracture surfaces that became coated with a thick oxide layer. Intergranular fracture was also found to be associated with large defects (Figure 5-13) in samples tested at 1550°C, indicating that local stress relief at the defects was accomplished by SCG even when the defects are below the tensile surface. Micrograph 5-12a shows intergranular fracture about a flake-like crack and micrographs 5-12b through 5-12d show intergranular fracture about subsurface pores.

Some unusual defects were observed (Figure 5-14) associated with large grains on the as-fired, as-formed tensile stressed face. Micrograph 5-14a shows some large grains that are similar to Figure 5-6 on a ONR-2 sample. Micrograph 5-14b appears to be a large subsurface grain.

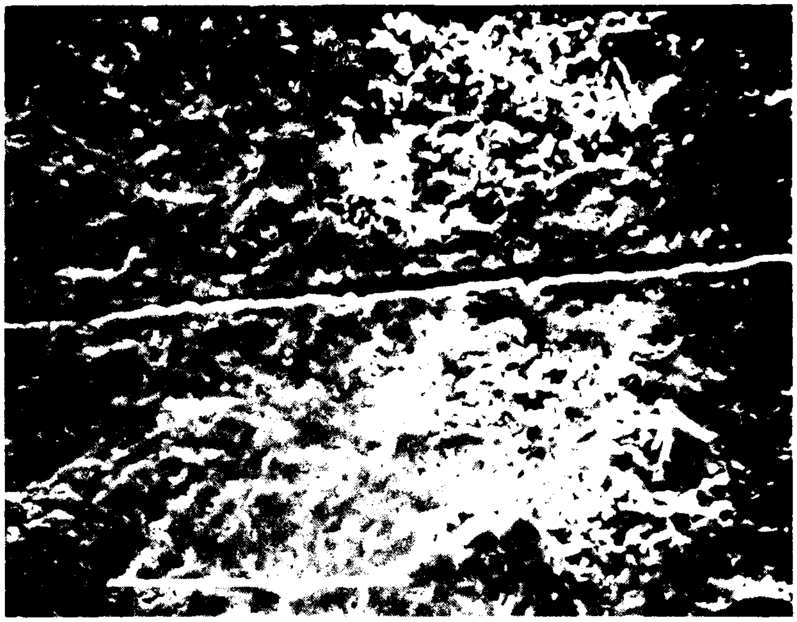

GROUP [illegible]06, SAMPLE [illegible]16, [illegible]50X

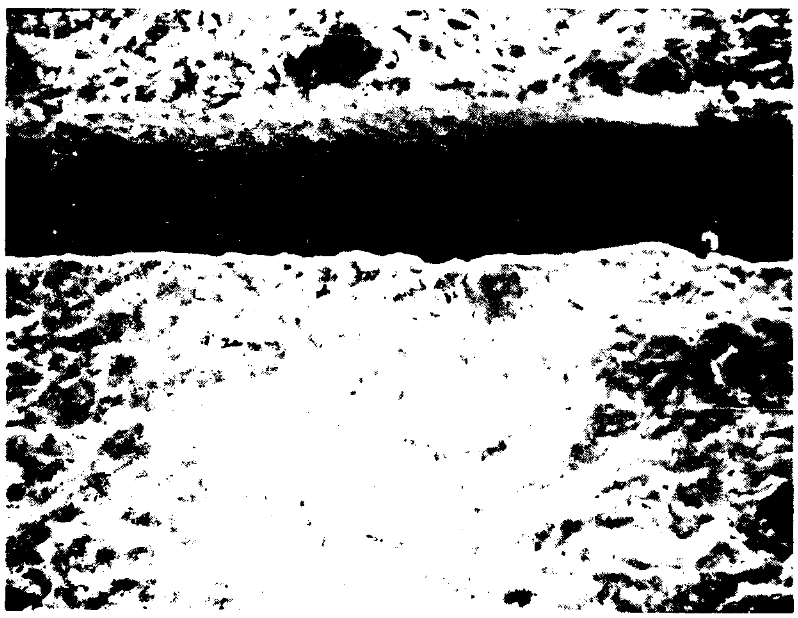

F-31351

[illegible] SAMPLE [illegible], [illegible]50X

Figure [illegible] [illegible] structure as the [illegible]

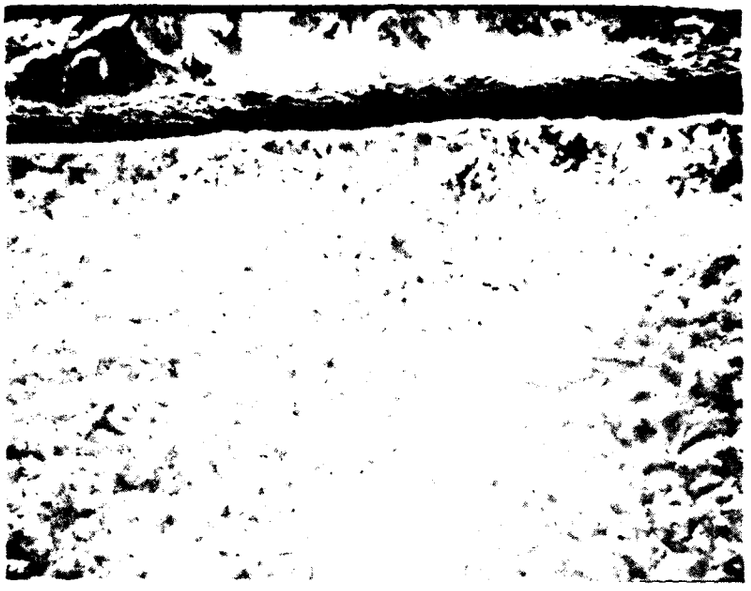

c. GROUP 106, SAMPLE 56, 350X

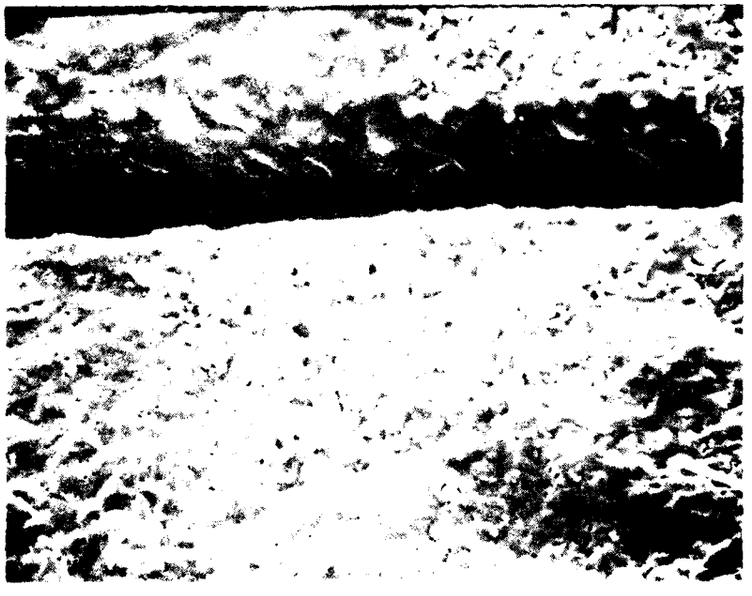

F 31352

d. GROUP 118, SAMPLE 102, 350X

Figure 5-12. (Continued)

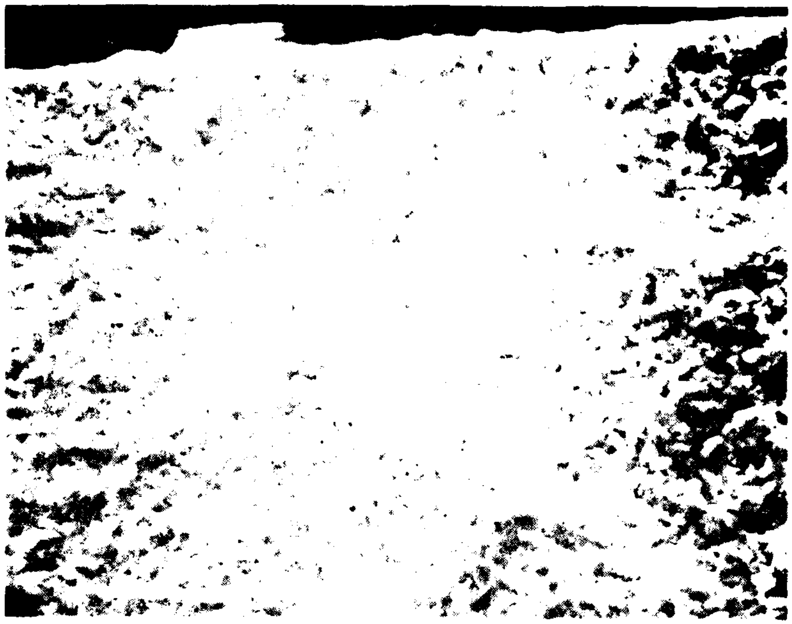

a. GROUP 114, SAMPLE 133, 350X

F-31353

b. GROUP 117, SAMPLE 168, 350X

Figure [illegible]. [illegible] Growth Associated With Defects
[illegible] Specimens

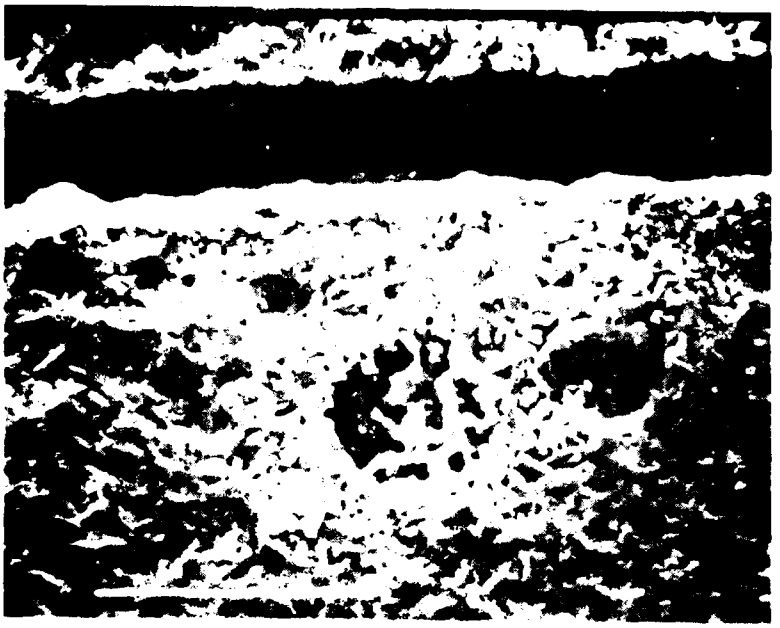

F 31354

a. GROUP 117, SAMPLE 73, 350X

F-31355

b. GROUP 116, SAMPLE 166, 350X

Figure [illegible] [illegible] Surface [illegible]

SECTION 6

CONCLUSIONS

Failures on tensile-stressed, as-fired samples were caused primarily by processing defects and did not appear to be associated with compositional changes (amount of sintering agent) in the material. At high testing temperatures (above 1340°C), the occurrence of processing defects appears to control strength, making it impossible to speculate on the effect of salt and oxidation during slow crack growth in these specimens.

Over the variety of conditions tested such as salt, oxidation, and their combinations, strength did not vary greatly. Therefore, the defects from processing represent the reasonable lower limit of strength under the imposed testing conditions. The determined strength values probably represent reasonable design data for components with as-fired, as-formed surfaces of similarly processed SASC. Since these strength values represent a reasonable lower limit for as-fired, as-formed surfaces of SASC, the potential is good for improvement by processing improvements to eliminate defects.

The observed defects were probably the result of processing since no variations in chemistry could be found at the defects. If the defects were formed by nondispersed binders or pressing die lubricants, these organics would be burned out during firing. Other defects such as surface cracks and flake-like cracks may be due to nonuniform density during powder pressing.

SASC continues to show promise as a viable engineering material. It will become more attractive for heat exchanger applications in aggressive environments as processing becomes more sophisticated.

SECTION 7

REFERENCES

1. Schwab, D. E. and D. M. Kotchick, "High Temperature Slow Crack Growth in Silicon Carbide (13 Oct 1976-13 Oct 1977)", AiResearch Report 78-15574, December, 1978.

2. K. D. McHenry, "Elevated Temperature Slow Crack Growth in Hot-Pressed and Sintered Silicon Carbide Ceramics," The Pennsylvania State University, PhD thesis, November, 1978.

3. J. A. Costello and R. E Tressler, Personal Communication.

4. E. H. Kraft and G. I Dooher, "Mechanical Response of High-Performance Silicon Carbides", Presented at 2nd International Conference on Mechanical Behavior of Materials, Boston, MA, August, 1976.

5. D. C. Larsen and G. C. Walther, "Property Screening and Evaluation of Ceramic Vane Materials", Report No. IITRI-D6114-17R-24, IIT Research Institute, Chicago, IL, October, 1977.

6. G. G. Trantina and C. A. Johnson, "Subcritical Crack Growth in Boron-Doped SiC", J. Amer. Ceram. Soc. 58 (7-8) 344-345 (1975).

7. A. G. Evans and F. F. Lange, "Crack Propagation and Fracture in Silicon Carbide", J. Mater. Sci, 10 (1975) 1659-64.

8. C. A. Johnson and S. Prochazka, "Investigation of Ceramics for High Temperature Turbine Components", Report NADC-75228-30, Naval Air Development Center, Warminster, PA, June 1977.

APPENDIX

HIGH-TEMPERATURE STRENGTH OF SINTERED α - SiC IN SALT AND OXIDIZING ENVIRONMENTS

HIGH TEMPERATURE STRENGTH OF SINTERED α-SiC IN SALT AND OXIDIZING ENVIRONMENTS

By:

D. E. Schwab and D. M. Kotchick

AiResearch Manufacturing Company of California

ABSTRACT

The flexure strength of as-fired and ground sintered α-SiC was determined at 20°C to 1620°C in air with and without ocean salt precoating, at strain rates of 0.3 to 90 μm/m•sec. Strength declined rapidly above 1400°C, particularly with slow straining, because of subcritical crack growth (SCG) of surface and subsurface flaws. At 20°C, preoxidation or salt precoating increased strength. Salting seemed to enchance SCG at 1200°C to 1400°C.

I. INTRODUCTION

Sintered α-SiC (SASC) is an attractive candidate for intricately-shaped parts that must withstand high stresses at temperatures of 1000 - 1700°C. In many instances, these parts will be subjected to oxidizing and/or ocean-salt-laden gases for extended times while stressed. Therefore, it is necessary to know whether slow crack growth (SCG) will occur in SASC at high temperatures. The weakening influence of SCG could be enhanced or retarded by oxidation and/or ocean salt deposits.

Although SCG has been detected in SiC grades containing free silicon[1-5], the cracking process is usually discontinuous and seems to be related primarily to the silicon phase rather than the SiC, especially near the melting point of silicon. In the very dense, hot-pressed grades of SiC containing Al_2O_3, SCG at low temperatures seems to be a moisture-related, stress-corrosion process, whereas SCG at high temperatures has been attributed to plastic flow of the softened grain boundary phase.[5-7] Tests of a dense, fine-grained ($\leq$10μm) β-SiC[6, 8, 9] revealed no SCG below 1500°C, except in water at room temperature, where SCG characteristics resembled those of hot-pressed SiC. However, SCG in β-SiC appeared to have occurred in 1600°C air. Limited tests of several grades of SiC [8, 10-13], have revealed that high-temperature exposure to air, helium, and salt-containing gases can improve their strength significantly[8, 10] by healing or rounding cracks and flaws. There have also been reports[14] of severe attack on hot-pressed and reaction-sintered grades of SiC immersed in molten Na_2SO_4, and of SCG in SASC oxidized at moderately high temperatures.[15]

Two sets of experiments, reported herein, were conducted to determine the extent and causes of SASC strength changes due to high temperatures, oxidation and hot corrosion by ocean salt. The strength of as-formed, as-fired surfaces were emphasized, because of the obvious advantages of net-shape fabrication of

SASC parts. In the first set of tests, a rather broad range of temperatures and surface conditions were explored to identify strength-limiting or strength-enhancing combinations. These critical surface-temperature combinations were investigated in greater detail in a second set of tests.

II. EXPERIMENTAL PROCEDURE

Several methods may be used to measure SCG in ceramics. Variable stress-rate flexure testing of bars[16] was selected for three reasons: (1) experimental simplicity, (2) ability to characterize natural microscopic flaw distributions in any surface or processing condition of interest, and (3) generation of strength data, a valuable by-product. Most other popular methods, such as double-torsion, double-cantilever-beam and indentation-flawed flexure tests, measure the effect of relatively large, artificial flaws and cannot provide information about existing flaw distributions which control strength.

MATERIAL PREPARATION

Billets of SASC* were prepared by cold-pressing and sintering. Flexure bars were each 2.5 x 5 x 44 mm. The specimens were cut from the top surface of SASC billets, leaving the top face as-formed and as-fired. The bottom face and sides of each sample were ground transversely with 200-grit diamond and then finished with 400-grit diamond. Long edges were lightly chamfered by hand with 200-grit diamond lapping compound. Width and thickness were within 0.13 mm of specified values. Ground surfaces were flat within 25 μm. Ground sides were parallel within 25 μm and were perpendicular to the faces within 1 deg. Visual, fluorescent dye-penetrant and radiographic inspections ensured that each specimen was free of defects greater than 0.5 mm long. Density, measured by the immersion method**, varied from 3.07 to 3.16 g/cc. Metallographic

* Carborundum Co.
**ASTM-C373-72

analysis revealed equiaxed grains averaging 8.6 m in diameter. The microstructure is shown in Figure 1. Samples were etched using hot oxalic acid.

For each test, specimens were selected at random from among the various billets, so that the usual batch-to-batch property variations due to composition and processing differences would influence all the test groups in the set in the same way. The surfaces of selected specimens (Table 1) were wiped with isopropanol and were subsequently treated to permit corrosion and oxidation effects to be evaluated. Some were oxidized by heating in air at 1260°C; some were coated with concentrated artificial ocean saltwater*** heated at 120°C to evaporate the water and then subjected to 900°C and 1260°C air in an electric furnace. Exposure times were chosen to ensure that oxidation passed the point of initial rapid weight gain with time. Experimental data of Costello and Tressler[17] provided guidance in this regard. The surface to be tested in tension faced upward during the oxidation or salt treatment. The samples were cooled slowly in the furnace.

FLEXURE TESTING

Flexure tests were conducted in a SASC floating-pin, 4-point bend fixture* having a 38 mm outer span and a 13 mm inner span. Loads were applied by a universal test machine† at varying speeds, through silicon carbide push rods. Loading rates, recorded autographically, were converted to strain rates by computation.

The fixture and specimen were contained within a silicon carbide element electric furnace§ which provided temperatures as high as 1620°C. Temperatures were monitored with a micro-optical pyrometer and were within 3°C of the reported value.

***ASTM-D1141-52 (without heavy metals)
†Instron Corporation
§W. P. Keith Company

Fracture surfaces of each specimen were examined under a low-magnification stereomicroscope to locate the fracture origin. Scanning electron microscope (SEM) photos were taken of selected specimens to further explore the strength-limiting flaws at the fracture origins.

III. RESULTS

The results of each group of replicate tests were plotted in Weibull form, as shown in Figure 2. The computed arithmetic mean strength, standard deviation, median strength and Weibull modulus (m) are shown. A least-squares straight line fit was used to compute m, as defined by the linear equation

$$\ln \ln [1/(1-P_f)] = m \ln \sigma + \ln \sigma_o \qquad (1)$$

where P_f is the estimated failure probability, σ is stress and σ_o is a constant. The results are summarized in Table 1.

Various strain rates were used to test groups of samples at a given surface condition and temperature. Results of these tests were plotted on a logarithmic scale as strength versus strain rate. The mean strength and strain rate for each group of data were fit to a straight line to obtain the slow crack growth exponent (n) defined by

$$V = AK^n \qquad (2)$$

and

$$(\sigma_1/\sigma_2)^{n+1} = \dot{\varepsilon}_1/\dot{\varepsilon}_2 \qquad (3)$$

where V is the crack growth rate, A is a constant, K is the stress intensity factor, and σ_1 and σ_2 are the strengths of samples tested at strain rates $\dot{\varepsilon}_1$ and $\dot{\varepsilon}_2$, respectively. Results are included in Table 1, and are plotted versus test temperature in Figure 3. Figure 4 shows some typical flaws at fracture origins. Samples that failed from flaws at the machined edges were eliminated from the analysis.

IV. DISCUSSION

These experiments provide data for the preliminary design of components with as-fired, as-formed surfaces. The test conditions were designed to explore material limitations and indicate probable strength-limiting mechanisms in light of related experiments by others. Accordingly, the statistical significance within each set may not be high. In particular, the calculated Weibull modulus (m) and stress intensity exponent (n) have not been determined at highly significant levels. Assumptions for the use of equation 3 have been met.[16]

Although the samples for sets A and B were specified and intended to be identical in composition and processing, room temperature tests indicate that set B was slightly weaker and less variable in strength than set A, as can be seen by comparing Group 28 with 1, and Group 30 with 7. These differences are considered to be normal batch-to-batch variations for SASC which may be due in part to differences in surface texture on the as-fixed, as-formed surfaces. At high temperatures, the differences in strength between A and B were further decreased.

The 20°C strength of as-fired surfaces was apparently improved by either pre-oxidation or by the salt-coating treatment. Comparing Group 28 with 30 and Group 1 with 11, it appears that the Weibull modulii are similar, although the mean strengths are quite different. This indicates that although the distribution of flaws is similar, their severity is less for the oxidized and salt-coated samples. Flaw-healing and/or blunting are likely mechanisms responsible for this behavior[8, 10, 12].

Testing temperature had the strongest influence upon strength. Figure 5 shows that mean strength declined markedly above 1400°C. The strength of SASC at 1620°C was reduced to about 50 percent of the value at 1300°C for samples that were strained slowly ($\dot{\epsilon} \approx 0.5$ m/m sec). The strength variation due to

intentional surface treatment differences was no greater than the standard deviation of strength within each group of identically-treated samples. The strength of SASC did not appear to be changed by any of the surface treatments used here, at least for the testing conditions and times that were imposed in these experiments.

Tests in dry N_2 indicate that apparent SCG at 20°C was probably humidity-related. The rate of SCG was also strongly influenced by test temperature, as shown in Figure 3. SCG increased (n decreased) markedly with increasing temperature in the range 1200 - 1400°C. Within that range, SCG was apparently enhanced by coating the as-fired SASC surfaces with ocean salt. Oxidation of as-fired surfaces seemed to have had less effect on SCG than did salt coating. Preoxidized, salt-coated surfaces showed the same trends as oxidized surfaces.

Figure 4 shows examples of surface and near-surface flaws which typically caused failure of specimens from all the groups tested. Except near the origin, cracks propagated transgranularly. Some subsurface defects were connected to the surface by small cracks and high porosity which effectively increased the size of the subsurface defect. Limited access of oxygen to those defects would encourage corrosion of the SiC in the subsurface defects by the molten salt. As temperature increases, greater amounts of oxygen are needed to passivate the SiC, and the reaction kinetics also favor more rapid corrosion[18]. The present SCG findings, especially in the 1200 - 1400°C regime, agree with this explanation. Therefore, it is likely that the pre-oxidation of as-fired surfaces retarded the SCG enhancement of the salt by filling interconnecting surface porosity with oxide, as well as by blunting crack-like surface defects.

Diamond-ground (untreated or salt-coated) surfaces showed little or no difference from the behavior of as-fired surfaces. This indicates that the diamond grinding may have introduced nearly the same size flaws as are found on the as-fired surfaces.

V. CONCLUSIONS

Sintered α-SiC (SASC) with as-formed, as-fired surfaces is limited in strength above 1400°C by surface and subsurface flaws ≈200 μm in size that appear to undergo slow (subcritical) crack growth (SCG) prior to rapid transgranular propagation. Strength declines rapidly above 1400°C, particularly under slow straining conditions. Strength of as-fired surfaces at 20°C was increased by high-temperature oxidation or coating with ocean salt, probably by blunting or healing of surface flaws.

The mechanism for SCG at high temperatures was not identified. The extent of SCG appeared to increase with increasing temperature. Salt-coating seemed to enhance SCG in the 1200 - 1400°C range except when samples were oxidized before salt-coating. The oxide layer probably served to bar entry of the salt into the defects.

ACKNOWLEDGEMENTS

The authors would like to acknowledge the support of the Office of Naval Research and Mr. Keith Ellingsworth during the course of this study.

SINTERED α = SiC FLEXURE TESTS

Set	Group No.	Qty.	Temperature (°C)	$\dot{\epsilon}$ (μm/msec)	Strength (MPa) Mean	SD	Weibull Exponent m	n
As-Fired Surface								
A	1	19	20	50	342	48	8	-
B	28	10	20	50	302	25	12	-
A	2	5	1060	2	392	42	8	-
A	3	5	1340	50	378	39	8	
A	4	6	1340	3	348	41	8	30
A	5	6	1620	60	234	25	8	
A	6	6	1620	1	183	19	9	15
As-Fired Plus Oxidized Surface								
B	29*	10	20	0.5	387	27	13	-
A	7	9	20	50	403	48	8	-
B	30	10	20	50	375	29	12	
B	31	9	20	0.5	347	34	7	53
B	32	5	1000	40	382	19	18	
B	33	10	1000	0.5	358	74	5	54
B	34	5	1275	50	374	52	6	
B	35	5	1275	4	361	61	15	48
B	36	5	1275	0.5	339	14	18	
B	8	8	1340	40	367	44	8	
A	9	9	1340	1	321	39	8	27
B	37	10	1550	30	325	52	6	
B	38	5	1550	3	301	30	7	14
B	39	10	1550	0.3	235	34	7	
A	10	4	1620	30	213	36	-	-
As-Fired Plus Salt-Coated Surface								
A	11	10	20	50	373	53	7	-
A	12	5	1060	5	370	30	10	-
B	40	8	1275	40	369	52	7	
B	41	8	1275	0.4	307	54	5	23
A	13	9	1340	50	390	40	9	
A	14	6	1340	6	356	59	5	12
A	15	9	1340	2	303	39	7	
B	42	7	1550	30	349	63	5	
B	43	8	1550	0.4	227	33	6	9
A	16	6	1620	30	227	21	10	
A	17	1	1620	2	183	-	-	17
A	18	5	1620	0.5	161	30	5	
As-Fired Plus Oxidized Plus Salt-Coated Surface								
B	44	7	1275	50	394	40	9	
B	45	8	1275	0.6	367	33	10	61
B	46	8	1550	30	332	39	8	
B	47	6	1550	0.3	247	37	6	15
Diamond-Ground Surface								
A	19	7	20	90	350	23	14	-
A	20	5	1340	90	383	43	7	-
A	21	1	1620	1	192	-	-	-
Ground Plus Salt-Coated Surface								
A	22	1	20	90	360	-	-	-
A	23	6	20	3	340	67	5	-
A	24	5	1340	40	360	58	5	
A	25	10	1340	2	334	59	5	38
A	26	5	1620	30	250	39	6	
A	27	5	1620	0.5	159	14	10	6

Note: For set A, oxidation cycle was 65h in 1260°C air; salt-coating cycle was 5h in 900°C air, followed by 16h in 1260°C air. For set B, oxidation cycle was 24h in 1260°C air; salt-coating cycle was 65h in 900°C air, followed by 65h in 1260°C air.

* Group 29 was tested in dry nitrogen; all other groups were tested in air.

REFERENCES

1. D. E. Schwab and H. A. Warren, "High-Temperature Slow Crack Growth in Silicon Carbide," Report No. 77-13571, AiResearch Manufacturing Co. of California.

2. A. Pietsch, "Coal-Fired Prototype High-Temperature Continuous-Flow Heat Exchanger," Report No. AF-684, Electric Power Research Institute, Palo Alto, CA, February 1978.

3. G. G. Trantina, "Fracture of a Self-Bonded Silicon Carbide," Ceramic Bulletin 57 (4)440-443 (1978).

4. R. W. Davidge, G. Tappin and J. R. McLaren, "Strength Parameters Relevant to Engineering Applications for Reaction Bonded Silicon Nitride and REFEL Silicon Carbide," Powder Metall. Int., pp. 110-114 (August, 1976).

5. K. D. McHenry and R. E. Tressler, "Subcritical Crack Growth in Silicon Carbide," J. Mater. Sci. 12, 1272-1278 (1977).

6. A. G. Evans and F. F. Lange, "Crack Propagation and Fracture in Silicon Carbide," J. Mater. Sci. 10 1659-64 (1975).

7. K. D. McHenry, T. M. Yonushonis and R. E. Tressler, "Low Temperature Subcritical Crack Growth in SiC and Si_3N_4, J. Amer. Ceram. Soc. 59 (5-6) 262-263 (1976)

8. C. A. Johnson and S. Prochazka, "Investigation of Ceramics for High Temperature Turbine Components," Report NADC-75228-30, Naval Air Development Center, Warminster, PA, June, 1977.

9. G. G. Trantina and C. A. Johnson, "Subcritical Crack Growth in Boron-Doped SiC," J. Amer. Ceram. Soc. 58 (7-8) 344-345 (1975).

10. F. F. Lange, "Healing of Surface Cracks in SiC by Oxidation," J. Amer. Ceram. Soc. 53(5) 290 (1970).

11. S. C. Singhal, "Corrosion-Resistant Structural Ceramic Materials for Gas Turbines," in Report No. MCIC-75-27, Battelle Memorial Institute, Columbus, Ohio, July 1974.

12. R. E. Wallace, "Ceramic Gas Turbine Engine Demonstration Program, Interim Report No. 4." Report No. 76-212188(4), AiResearch Mfg. Co. of Arizona, Phoenix, AZ, March 1977.

13. C. A. Johnson, "Crack Blunting in Sintered SiC," in Fracture Mechanics of Ceramics, Vol. 3. (ed. by R. C. Bradt, et. al.,) Plenum Press, New York, 99-111 (1973).

14. R. E. Tressler, M. D. Meiser and T. Yonushonis, "Molten Salt Corrosion of SiC and Si_3N_4 Ceramics," J. Amer. Ceram. Soc. 59 (5-6) 278-279 (1976).

15. K. D. McHenry "Elevated Temperature Slow Crack Growth in Hot-Pressed and Sintered Silicon Carbide Ceramics," The Pennsylvania State University, PhD thesis, Nov. 1978.

16. R. W. Davidge, J. R. McLaren and G. Tappin, "Strength-Probability-Time (SPT) Relationships in Ceramic," J. Mater. Sci. 8 1699-1705 (1973).

17. J. A. Costello and R. E. Tressler, Personal Communication.

18. D. W. McKee and D. Chatterji, "Corrosion of Silicon Carbide in Gases and Alkaline Melts," J. Amer. Ceram. Soc. 59 (9-10) 441-444 (1976).

FIGURE CAPTIONS

Figure 1. Sintered Alpha SiC Microstructure

Figure 2. Weibull Plot

Figure 3. Temperature Dependence of Slow Crack Growth Exponent (n) in Sintered α-SiC

Figure 4. Typical Surface (a) and Subsurface (b) Flaws

Figure 5. Temperature Dependence of Mean Flexural Strength for Sintered α-SiC

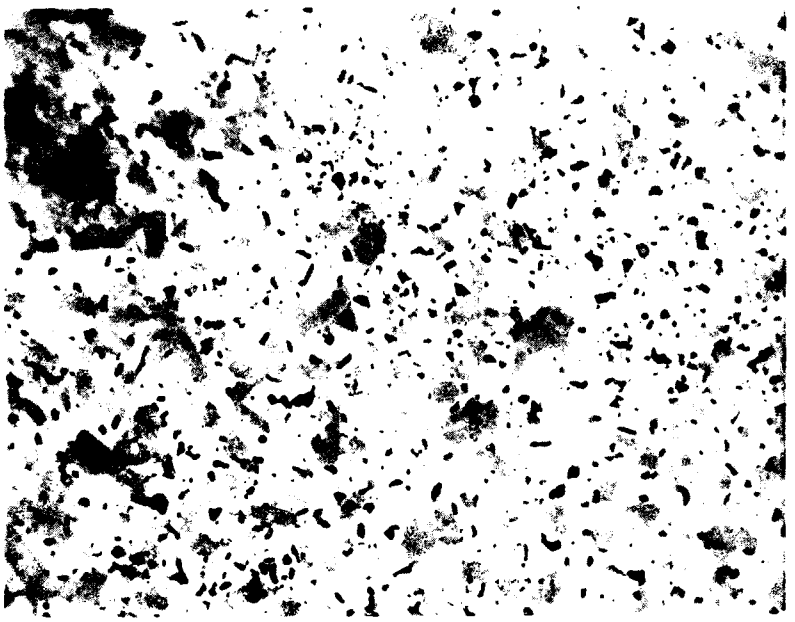

500 X

F-28107

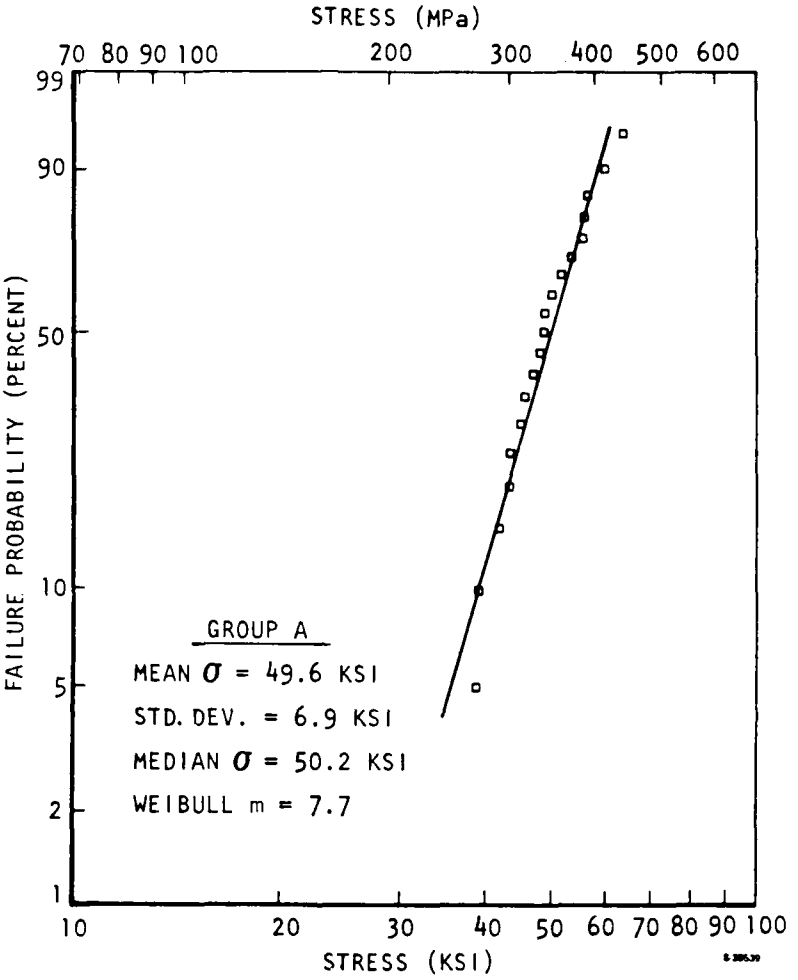
STRESS (MPa)
70 80 90 100
200
300
400
500
600
99
90
50
10
5
2
1
FAILURE PROBABILITY (PERCENT)
GROUP A
MEAN σ = 49.6 KSI
STD. DEV. = 6.9 KSI
MEDIAN σ = 50.2 KSI
WEIBULL m = 7.7
10
20
30
40
50
60
70
80
90
100
STRESS (KSI)

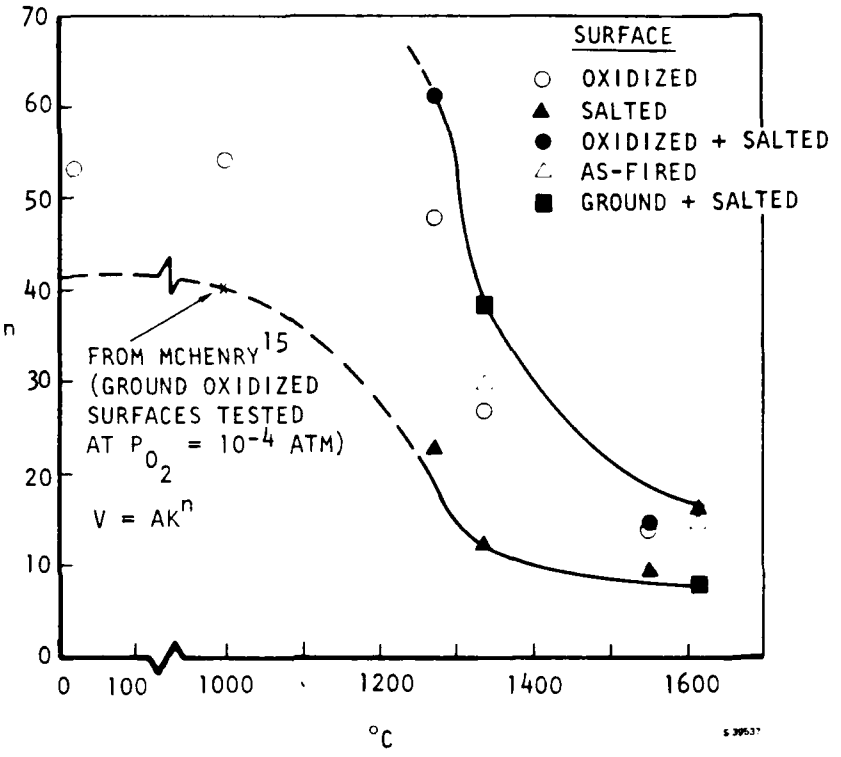
SURFACE
OXIDIZED
SALTED
OXIDIZED + SALTED
AS-FIRED
GROUND + SALTED
FROM MCHENRY[15]
(GROUND OXIDIZED
SURFACES TESTED
AT $P_{O_2} = 10^{-4}$ ATM)
$V = AK^n$
n
°C
0
10
20
30
40
50
60
70
0
100
1000
1200
1400
1600

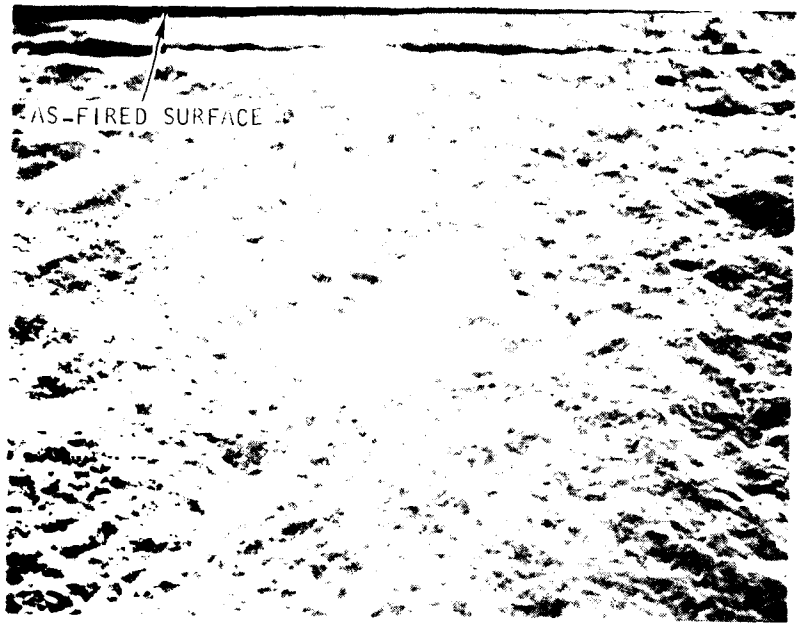

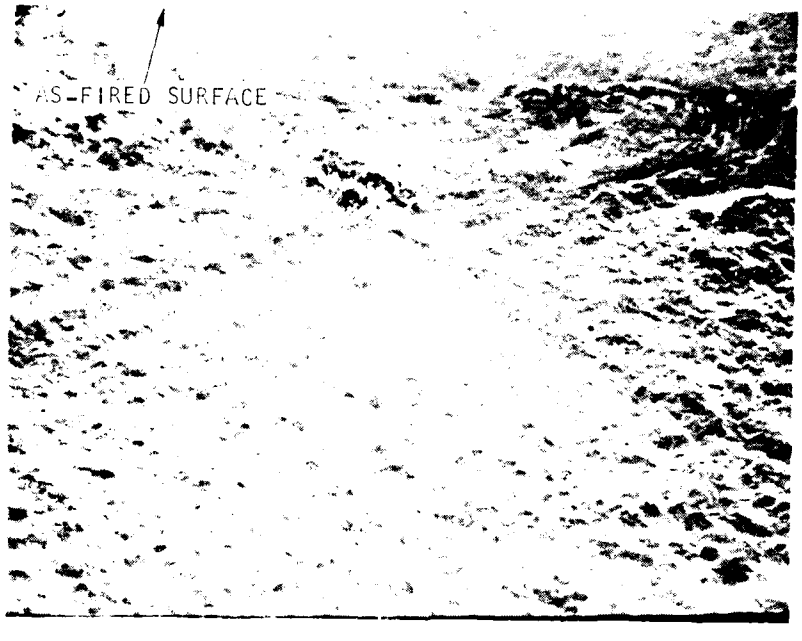

F-31385

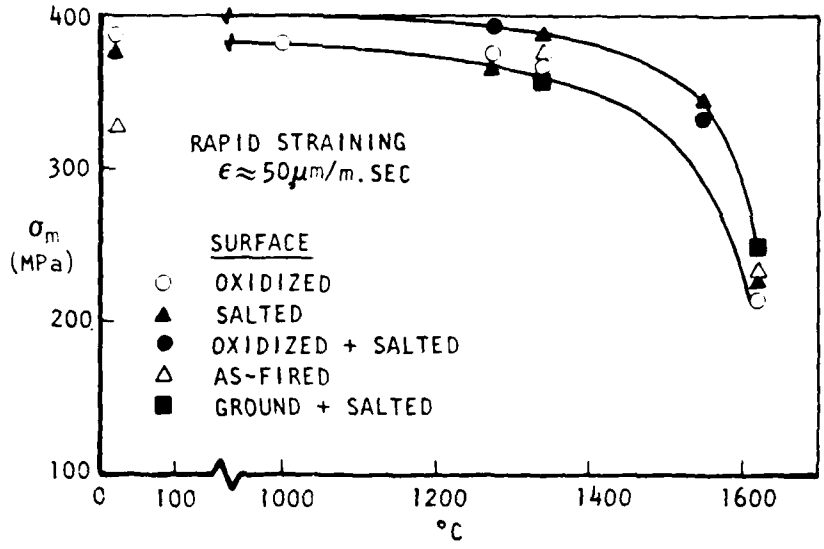
400
300
200
100
σ_m (MPa)
RAPID STRAINING
$\epsilon \approx 50\mu m/m.SEC$
SURFACE
OXIDIZED
SALTED
OXIDIZED + SALTED
AS-FIRED
GROUND + SALTED
0
100
1000
1200
1400
1600
°C

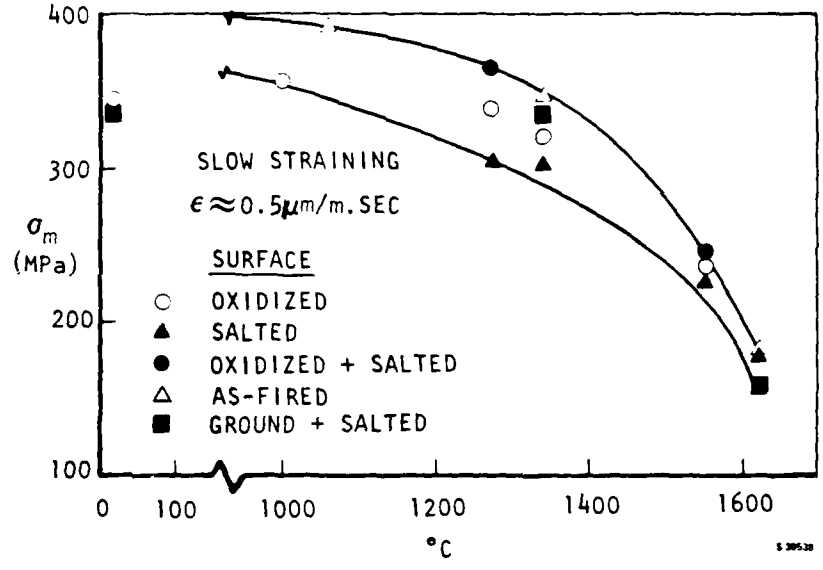
400
300
200
100
σ_m (MPa)
SLOW STRAINING
$\epsilon \approx 0.5\mu m/m.SEC$
SURFACE
OXIDIZED
SALTED
OXIDIZED + SALTED
AS-FIRED
GROUND + SALTED
0
100
1000
1200
1400
1600
°C

DISTRIBUTION LIST

CERAMICS APPLIED RESEARCH

	No. Copies
Office of Naval Research 800 N. Quincy Street Arlington, VA 22217	
Attn: Power Program, M. Keith Ellingsworth	3
Technology Group	1
Metallurgy & Ceramics Program, Dr. A. Diness	1
Defense Documentation Center Bldg. 5 Cameron Station Alexandria, VA 22314	12
Naval Research Laboratory 4555 Overlook Ave. Washington, DC 20390	
Attn: Technical Information Division	12
Ceramics, Code 6360, Mr. Roy Rice	1
US Naval Post Graduate School Monterey, CA 93940	
Attn: Dept. of Mechanical Engineering	1
US Naval Academy Annapolis, MD 21402	
Attn: Dept. of Mechanical Engineering	1
Office of Naval Research Branch Office 495 Summer Street Boston, MA 02210	
Attn: Dr. F. S. Gardner	1
Office of Naval Research Branch Office 536 South Clark Street Chicago, IL 60605	
Attn: Mr. G. Sandos	1
Office of Naval Research San Francisco Area Office 1 Hallidie Plaza, Suite 601 San Francisco, CA 94102	
Attn: Dr. P. A. Miller	1

DISTRIBUTION LIST (Continued)

	No. Copies
Naval Air Systems Command Jefferson Plaza Washington, DC 20360 Attn: Propulsion Administrator, Code 330	1
Naval Sea Systems Command Crystal Plaza Washington, DC 20360 Attn: Ship Main Propulsion & Energy Br., Code 0331 Materials and Mechanics Division, Code 0351	1 1
Naval Ship Engineering Center National Center Washington, DC 20362 Attn: Heat Exchanger Section, Code 6145F	1
Naval Ship R&D Center Annapolis, MD 21402 Attn: Power Systems Division Gas Turbine Branch Material Dept., Code 28	1 1 1
Army Research Office P.O. Box 12211 Research Triangle Park, NC 27709 Attn: Mr. James J. Murray	1
Air Force Office of Scientific Research Bolling Air Force Base Washington, DC 20332 Attn: Directorate of Aerospace Sciences	1
National Science Foundation 1800 G Street NW Washington, DC 20550 Attn: Div. of Materials Research, Ceramics	1
Energy Research & Development Administration 20 Massachusetts Ave. NW Washington, DC 20545 Attn: Div. of Conservation Research & Technology Heat Engines and Components Div. of Fossil Energy, Advanced Power, Mr. Carey Kinney Mr. Steve Wander	 1 1 1
Naval Weapons Center China Lake, CA 93555 Attn: Mr. Bill Thielbar, Code 3161	1

DISTRIBUTION LIST (Continued)

	No. Copies
University of Arizona Aerospace & Mechanical Engineering Dept. College of Engineering Tucson, AZ 85721 Attn: Professor Don McEligot	1
University of Rhode Island College of Engineering Kingston, RI 02881 Attn: Professor P. Gielissi	1
Georgia Institute of Technology School of Ceramic Engineering Atlanta, GA 30332 Attn: Professor Joseph Pentecost	1
National Aeronautics Space Administration 105-1 Cleveland, OH 44135 Attn: Mr. Joseph R. Stephens	1
SEALOL Corp. P.O. Box 2158 Providence, RI 02905 Attn: Mr. Walter Meyer	1
Crane Packing Co. 6400 Oakton Street Morton Grove, IL 60053 Attn: Mr. Joe Trytek	1
Carborundum Co. Graphite Products Division P.O. Box 577 Niagara Falls, NY 14302 Attn: Mr. Ervin Ruppel	1
Norton Company Industrial Ceramics Division 1 New Bond Street Worcester, MA 01606 Attn: Mr. Wray	1
Mechanical Technology Inc. 968 Albany Shaker Rd. Latham, NY 12110 Attn: Dr. Donald Wilcock	1

DISTRIBUTION LIST (Continued)

	No. Copies
Hague International 3 Adams Street South Portland, ME 04106 Attn: Dr. John W. Bjerklie	1
Solar Turbines International 2200 Pacific Highway P.O. Box 80966 San Diego, CA 92138 Attn: Dr. M. E. Gulden	1
Black & Veatch Consulting Engineers P.O. Box 8405 Kansas City, MO 64114 Attn: Dr. J. C. Grosskreutz	1
Physical Chemistry Lab. Corporate Research & Development General Electric Company Schenectady, NY 12301 Attn: Dr. Robert G. Fullman	1
ITT Research Institute Mechanics of Materials Division Chicago, IL 60616 Attn: Mr. David Larson	1
Energy Research & Generation, Inc. Lowell & 57th Street Oakland, CA 94608 Attn: Dr. Glen Benson	1